nature communications

Article

https://doi.org/10.1038/s41467-025-60736-y

Fumarylacetoacetate hydrolase targeted by a *Fusarium graminearum* effector positively regulates wheat FHB resistance

Received: 11 January 2024

Accepted: 29 May 2025

Published online: 01 July 2025

Check for updates

Shengping Shang[1,2], Yuhan He[1], Ruihua Zhao[1,3], Hanqi Li[1,4], Ying Fang[1,5], Qianyong Hu[1], Yujin Fan[1], Yiwei Wang[1,6], Xishi Zhou[1], Penghao Wang[3,7], Xiaoping Xing[2] & Cui-Jun Zhang[1]

Fusarium head blight (FHB), caused by *Fusarium graminearum* is a devastating disease that affects global wheat production. *F. graminearum* encodes many effector proteins; however, its virulence mechanisms are poorly understood. In this study, we identify a secretory effector candidate (FgEC10) that is essential for the virulence of *F. graminearum*. FgEC10 interacts strongly with wheat fumarylacetoacetate hydrolase (TaFAH) and accelerates its degradation via the 26S proteasome pathway. In addition, we show that TaFAH interacts with proteasome 26S subunit, non-ATPases 12 (TaPSMD12) and that FgEC10 enhances the interaction between TaFAH and TaPSMD12. RNA silencing or overexpression of *TaFAH* in wheat plants shows that *TaFAH* positively regulates wheat FHB resistance. Overexpression of *TaFAH* promotes the expression of genes associated with disease resistance and the heading period. Metabolomic analysis reveals that overexpression of *TaFAH* increases the levels of several amino acids in wheat, and exogenous application of some of these amino acids show an increase in *F. graminearum* resistance in the wheat spike and seedling. Collectively, our study reveals a pathogenic mechanism and provides a valuable gene resource for improving FHB resistance and promoting heading in wheat.

Fusarium head blight (FHB), caused by *Fusarium graminearum*, is a destructive disease that affects wheat and barley worldwide[1]. FHB outbreaks often lead to staggering financial losses, amounting to billions of dollars[1]. In addition to causing severe reductions in wheat yield and grain quality, *F. graminearum* generates many harmful mycotoxins, such as deoxynivalenol (DON), 3-acetylated (3-ADON) or 15-acetylated derivatives (15-ADON), and nivalenol (NIV), which inhibit the synthesis of human and animal cell proteins and destroy the hematopoietic and immune systems[2]. Planting resistant wheat cultivars is an effective and environmentally friendly method for controlling FHB. However, there are limited sources of FHB resistance among wheat cultivars; only two resistance genes, *Fhb1* and *Fhb7*, have been identified in wheat, neither of which provides complete resistance[3–5]. It is crucial to investigate the pathogenic mechanisms of *F. graminearum* at the molecular level to provide a theoretical basis for developing new prevention and control strategies to manage this disease effectively.

[1]Shenzhen Branch, Guangdong Laboratory of Lingnan Modern Agriculture, Key Laboratory of Synthetic Biology, Ministry of Agriculture and Rural Affairs, Agricultural Genomics Institute at Shenzhen, Chinese Academy of Agricultural Sciences, Shenzhen, China. [2]College of Plant Protection, Henan Agricultural University, Zhengzhou, China. [3]Centre for Crop and Food Innovation, Food Futures Institute, School of Agriculture Science, Murdoch University, Perth, WA, Australia. [4]College of Agriculture, Shanxi Agricultural University, Taigu, Shanxi, China. [5]College of Life Science and Technology, Huazhong Agricultural University, Wuhan, China. [6]College of Data Science, Taiyuan University of Technology, Taiyuan, China. [7]School of Medical, Molecular and Forensic Sciences, College of Science, Health, Engineering and Education, Murdoch University, Murdoch, WA, Australia. e-mail: zhangcuijun@caas.cn

Fusarium graminearum has been identified as a hemibiotrophic fungus[6]. During the initial penetration stage, compound appressoria and infection cushions are produced. Consequently, the invasive hyphae generate bulbous, irregular growths visually distinct from epiphytic hyphae. Subsequently, the fungus multiplies intracellularly after the induction of plant tissue death. Blight occurs in whole wheat heads when infected tissue spreads from the initial source to nearby spikelets via the rachis. Over the last decade, most global researchers have focused on the intracellular proteins of *F. graminearum* and have identified over 200 virulence genes that affect its ability to colonize wheat and other hosts. These pathogenic factors include transcription factors, proteins involved in signaling transduction pathways, enzymes related to primary metabolism, and catalytic enzymes involved in DON synthesis[7–10].

In addition to intracellular proteins, biotrophic and hemibiotrophic pathogens deliver effector proteins into the plant apoplast to modulate plant defenses[11]. During pathogen-plant interactions, plants take advantage of pattern recognition receptors (PRRs) located on cell surfaces to recognize pathogenic cell surfaces or secreted conserved pathogen-associated molecular patterns (PAMPs). This activates various immune responses, such as hormone signaling, calcium ion flow, mitogen-activated protein kinases, and phytoalexins[12,13]. However, successful phytopathogens release numerous effectors to overcome host immune responses[14,15]. For example, the LysM effector, Ecp6, prevents chitin-triggered immunity in plants[16], *Ustilaginoidea virens* secretes a family of phosphatases that stabilize the negative immune regulator OsMPK6 and suppress plant immunity[17], and the *Phytophthora sojae* RXLR effector Avh238 destabilizes soybean type2 GmACSs to suppress ethylene biosynthesis and promote infection[18]. *F. graminearum* encodes a large number of effector proteins, some of which are crucial for its ability to cause disease[19–22]. However, little is known about the host targets and virulence mechanisms of *F. graminearum* effector proteins.

The 26S is a conserved pathway for non-lysosomal protein degradation. In the process of protein degradation by the 26S proteasome pathway, the substrate is first ubiquitinated by E1–E3 ligases directly or indirectly, using shuttle proteins[23]. The 26S proteasome comprises two primary subcomplexes: the 19S regulatory complex and the 20S core complex. The 19S regulator consists of a lid and a base-like structure. The lid is composed of several PSMD (proteasome 26S subunit, non-ATPases) proteins and provides the binding sites for substrates[24]. The proteasome operates by binding ubiquitylated proteins to the 19S regulatory complex and then catalyzes them with the 20S core complex to control cellular protein levels[25]. The 26S proteasome system plays a crucial role in plant immunity, and disruption of this system is an effective way for plant pathogens to attack their hosts. Multiple bacterial effectors regulate target protein degradation via the ubiquitin–proteasomal pathway[26,27]. For instance, the Pi06432 effector of *P. infestans* targets StUDP to disrupt proteasomal homeostasis by degrading StRPT3b[28]. The *Magnaporthe oryzae* AvrPiz-t effector interacts with the rice RING-type E3 ligases, APIP6 and APIP10, impeding their ubiquitin ligase activity and promoting their destruction[29,30]. However, little is known about whether effector proteins can regulate the interactions of the PSMDs with target proteins.

Bread wheat is an allohexaploid crop ($2n = 6x = 42$, AABBDD), in which most genes have six copies in the A, B, and D subgenomes, resulting in functional redundancy and making it challenging to discover new resistance genes[31]. Pathogen effectors serve as valuable molecular probes to uncover new components of host immunity[32]. A better understanding of pathogen effector biology has led to new strategies for creating broad-spectrum disease-resistant crops. For instance, *Puccinia striiformis* f. sp. *tritici* effector PsSpg1 targets the wheat receptor-like cytoplasmic kinase TaPsIPK1, and inactivation of TaPsIPK1 confers broad-spectrum resistance to rust pathogens without affecting agronomic traits[33]. *U. virens* secretes a cytoplasmic effector that binds to the rice scaffold protein, OsRACK1A. Overproduction of OsRACK1A leads to reactive oxygen species (ROS) production, resulting in floral resistance in *U. virens* without any yield reduction in rice[34]. The rice susceptibility genes SWEETs are targeted by the transcription activator-like (TAL) effectors of *Xanthomonas oryzae* pv. *Oryzae*[35]. The edition of TAL effector-binding sites in the *SWEET* promoter region achieves broad-spectrum resistance against *X. oryzae* pv. *Oryzae*[36].

In the present study, we identified a *F. graminearum* effector, FgEC10, specifically up-regulated during plant infection. Gene deletion confirmed that *FgEC10* is a crucial virulence factor in wheat head infections. FgEC10 suppresses plant immunity-related gene expression, ROS burst, and callose deposition in *Nicotiana benthamiana*. Additionally, FgEC10 targets wheat fumarylacetoacetate hydrolase (TaFAH) and promotes its degradation via the 26S proteasome pathway. TaFAH is bound to the 26S proteasome regulatory subunit TaPSMD12, and FgEC10 enhanced the TaFAH-TaPSMD12 interaction, accelerating TaFAH degradation. Overexpression of *TaFAH* resulted in increased wheat resistance to *F. graminearum* and earlier heading. Transcriptomic analysis indicated that overexpression of *TaFAH* promoted the expression of genes involved in disease resistance and wheat heading. Further metabolome analysis showed that TaFAH overproduction increased the content of several amino acids. Exogenous application of these amino acids improved wheat head and seedling resistance to *F. graminearum*. Overall, our study revealed a previously unknown mechanism of fungal pathogen infection and identified gene resources for increasing wheat resistance to *F. graminearum*, with consequent improvement in heading period.

Results

FgEC10 contributes to the virulence of *F. graminearum*

To identify the pathogenic effector of *F. graminearum*, we employed a bioinformatics pipeline to predict putative candidate effectors (Supplementary Fig. 1). This approach enabled the identification of 148 candidate effector proteins (Supplementary Data 1). Leveraging transcriptomic data, we selected the top 10 genes exhibiting the most specific and significant upregulation during *F. graminearum* infection of wheat (Supplementary Fig. 1b) for subsequent gene knockout experiments (Supplementary Fig. 2). Pathogenicity analysis demonstrated that several of these effectors play critical roles in pathogenesis[37] (Supplementary Fig. 3). The virulence of *F. graminearum effector candidate 10* (*FgEC10*, *FGRAMPH1_01T21317*) mutants was significantly reduced during infection of wheat heads (Supplementary Fig. 3). The expression of *FgEC10* transcripts was characterized by RT-qPCR assay, which was negligible at 0 h post-infection (hpi). However, there was a substantial increase in their accumulation (approximately 60-fold) during the cushion-mediated penetration stage (24 and 48 hpi) (Supplementary Fig. 4).

The *FgEC10* mutation did not affect colony morphology or growth rate of *F. graminearum* on potato dextrose agar (PDA) plates (Fig. 1a, b; Supplementary Fig. 5). Upon infection of wheat heads, Δ*FgEC10*-6 and Δ*FgEC10*-12 mutants showed less virulence than the wild-type (WT) strain (Fig. 1c). The disease index on cultivar JiMai22 exhibited a reduction of 40.7% and 41.1% for Δ*FgEC10*-6 and Δ*FgEC10*-12, respectively, in comparison to that of the WT (Fig. 1d). Moreover, qPCR analysis of genomic DNA extracted from infected wheat showed that fungal biomass was significantly reduced in wheat infected with Δ*FgEC10* mutants compared with WT (Fig.1e). Furthermore, wheat heads inoculated with Δ*FgEC10* mutants exhibited approximately 30% less DON content compared to those inoculated with the WT (Fig. 1f). Nevertheless, the deletion of *FgEC10* had no impact on the DON production of *F. graminearum* in liquid trichothecene biosynthesis (LTB) medium (Supplementary Fig. 6a). The *TRI1*, *TRI5*, and *TRI6* genes are essential for trichothecene biosynthesis and DON production in *F. graminearum* (Chen et al. [1]). Their expression levels remained

https://doi.org/10.1038/s41467-025-60736-y

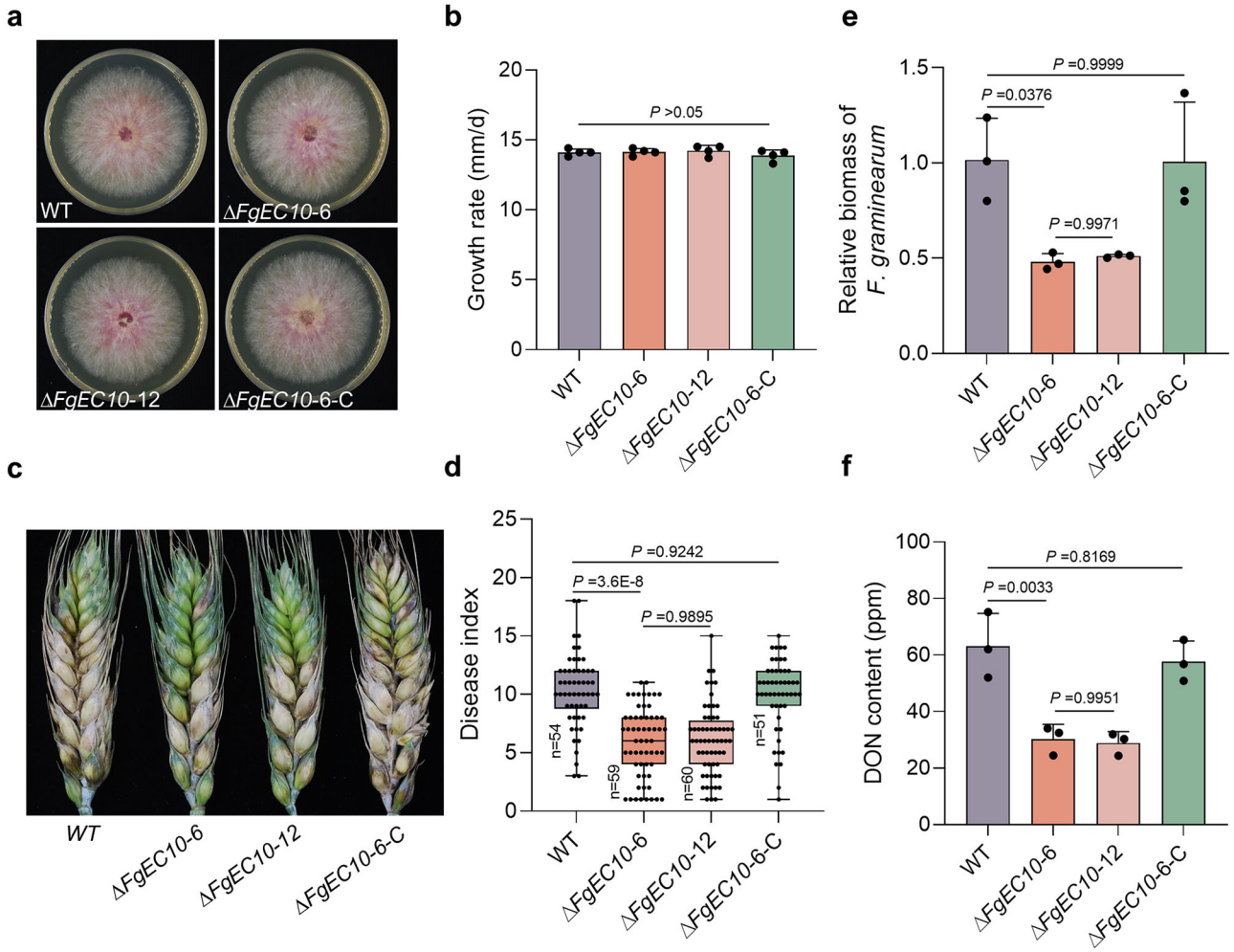

Fig. 1 | FgEC10 is required for *Fusarium graminearum* virulence in wheat heads. **a** Colony morphology of wild-type (WT), Δ*FgEC10* mutants (Δ*FgEC10*-6 and Δ*FgEC10*-12), and the complementary strain (Δ*FgEC10*-6-C) on PDA plates 5 days post-incubation. **b** Column diagrams showing the growth rates of the WT, Δ*FgEC10*-6, Δ*FgEC10*-12, and Δ*FgEC10*-6-C strains. Data represent four biological replicates. **c** Disease symptoms of wheat heads infected with the WT, Δ*FgEC10*-6, Δ*FgEC10*-12, and Δ*FgEC10*-6-C strains 14 days post-inoculation. **d** The disease indexes of WT, Δ*FgEC10*-6, Δ*FgEC10*-12, and Δ*FgEC10*-6-C strains on wheat. In the box plots: center line, median; box, interquartile range; whiskers, 1.5× interquartile range; and point, the disease index for each head. **e** Relative fungal biomass was measured using qPCR of DNA isolated from the same set of wheat plants as shown in (c). **f** The DON content in diseased wheat spikelets inoculated with WT, Δ*FgEC10*-6, Δ*FgEC10*-12, and Δ*FgEC10*-6-C strains. In (**d**–**f**), data are presented as mean ± SD from three independent replicates, one-way ANOVA test between WT and mutants.

unaltered in the Δ*FgEC10* mutants during infection of wheat heads (Supplementary Fig. 6b). The above results indicate that deletion of *FgEC10* does not influence *F. graminearum* DON production. Consequently, the reduction in DON content observed in wheat spikes may be attributed to a reduction in the number of infected spikelets throughout the spike. The complementary strain completely restored the pathogenic defect of the Δ*FgEC10*-6 mutant (Fig. 1c–f). Notably, both the Δ*FgEC10* and the WT strains produced the infection cushion normally (Supplementary Fig. 7). Thus, these results demonstrate that the function of FgEC10 is critical for *F. graminearum* to infect the wheat head and that FgEC10 may act as an effector during plant infection.

FgEC10 is delivered into host cells and suppresses basal immune responses

FgEC10 is a small protein that is predicted to contain a signal peptide (SP) at the N-terminus, and no other domains have been reported in FgEC10. Phylogenetic analyses using the FgEC10 protein sequence showed that the FgEC10 homologs are widely present in *Fusarium* species (Supplementary Fig. 8). We examined the accumulation of FgEC10 in the culture filtrates to determine whether FgEC10 was secreted into the extracellular compartment. FgEC10-GFP was detectable in the culture filtrate; however, the GFP control could not be detected under the same conditions (Fig. 2a). It was inferred that FgEC10 could be secreted extracellularly from *F. graminearum* cells. Furthermore, a coleoptile penetration assay was performed to confirm secretion. After inoculation of wheat coleoptile cells with strains expressing FgEC10-GFP or the GFP control, a GFP signal was detected in wheat cells incubated with the FgEC10-GFP strain but not in cells incubated with the GFP strain (Fig. 2b). These findings suggest that FgEC10 translocates from *F. graminearum* to plant cells during infection.

We analyzed the effect of FgEC10 on ROS and callose accumulation in *N. benthamiana* leaves in response to flg22 or chitin treatment to examine its influence on plant basal immunity. Compared with GFP, transient expression of FgEC10 significantly suppressed ROS burst and callose accumulation in *N. benthamiana*. (Fig. 2c–e). We assessed the expression of genes related to plant immune responses to investigate the effects of FgEC10 on basal wheat defense. Wheat heads inoculated with *FgEC10*-deletion mutants exhibited markedly elevated transcription levels of immunity-related genes, including *TaPR5* and *TaMAPK3*, compared to those inoculated with the WT strain (Fig. 2f). These findings suggested that FgEC10 functions as an immune suppressor in plant cells.

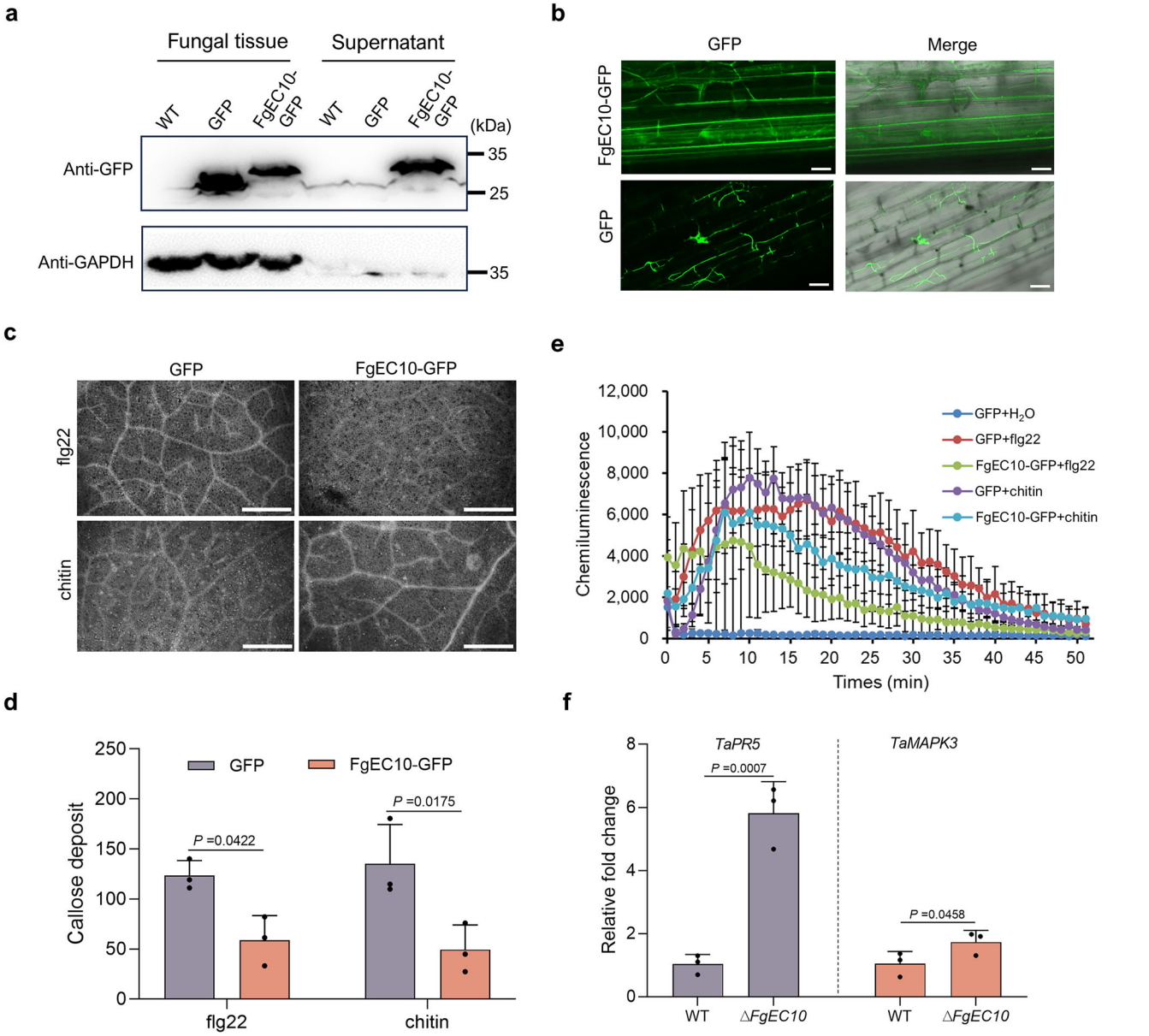

Fig. 2 | *F. graminearum* delivers FgEC10 protein into wheat cells and suppresses plant basal immunity. a FgEC10-GFP protein was detected in the total proteins of *F. graminearum* and culture filtrate using western blot analysis. The WT and GFP-transformed strains served as negative controls, and GAPDH protein levels were used as the internal control. **b** GFP signals in plant cells were examined. Wheat coleoptiles were infected with the indicated strains expressing GFP or FgEC10-GFP. Bar, 20 μm. **c** Callose deposition in *N. benthamiana* leaves expressing GFP or FgEC10-GFP after elicitation by flg22 or chitin. Bar, 1 mm. **d** The number of calloses in (**c**) from three biological replicates. **e** ROS accumulation induced by flg22 or chitin in *N. benthamiana* leaves expressing GFP or FgEC10-GFP. Data from six to eight biologically independent samples. **f** Transcript levels of *TaPR5* and *TaMAPK3* were evaluated in wheat heads inoculated with WT or Δ*FgEC10* mutant. The *TaACT* gene was used for normalization. All the data are presented as means ± SD from three independent replicates (one-tailed Student's *t*-test).

FgEC10 interacts with wheat TaFAH

To further elucidate the role of FgEC10 in wheat infection, a fusion construct pGBKT7-FgEC10$^{\Delta SP}$ was utilized as the bait to screen a prey yeast two-hybrid (Y2H) library. Ten potential interaction clones were identified after screening four times over the library (Supplementary Data 2). Subsequent point-to-point identification showed that only the TaFAH$^{81\text{-}427}$ (fumarylacetoacetate hydrolase, TaFAH, TraesCS6A03G0386400.1) interacted with FgEC10 (Fig. 3a). To further identify FgEC10-interacting proteins, we transiently expressed FgEC10-GFP in tobacco leaves and performed IP-MS assays. In two biological replicates of the IP-MS assays, NtFAH was identified once, suggesting that FAH is a possible target protein of FgEC10 (Supplementary Data 3). Furthermore, we demonstrated that full-length TaFAH co-pulled down with FgEC10, but not with MBP (Fig. 3b and Supplementary Fig. 9). In the luciferase complementation imaging (LCI) assay, a luminescence signal was observed in the leaves expressing FgEC10-cLuc combined with TaFAH-nLuc. In contrast, no signal was detected for any of the other three combinations, namely FgEC10-cLuc/nLuc, FgEC10/TaFAH-nLuc, and cLuc/nLuc (Fig. 3c). Subsequently, it was found that TaFAH-Flag co-immunoprecipitated with FgEC10-GFP but not with GFP using the co-immunoprecipitation (Co-IP) assay (Fig. 3d), indicating the interaction of FgEC10 and TaFAH in vivo. In addition, we conducted a bimolecular fluorescence complementation assay to determine the location of these interactions. GFP signals were detected within the cytoplasm of epidermal cells in *N. benthamiana* leaves infiltrated with FgEC10-YFPC and TaFAH-YFPN

https://doi.org/10.1038/s41467-025-60736-y

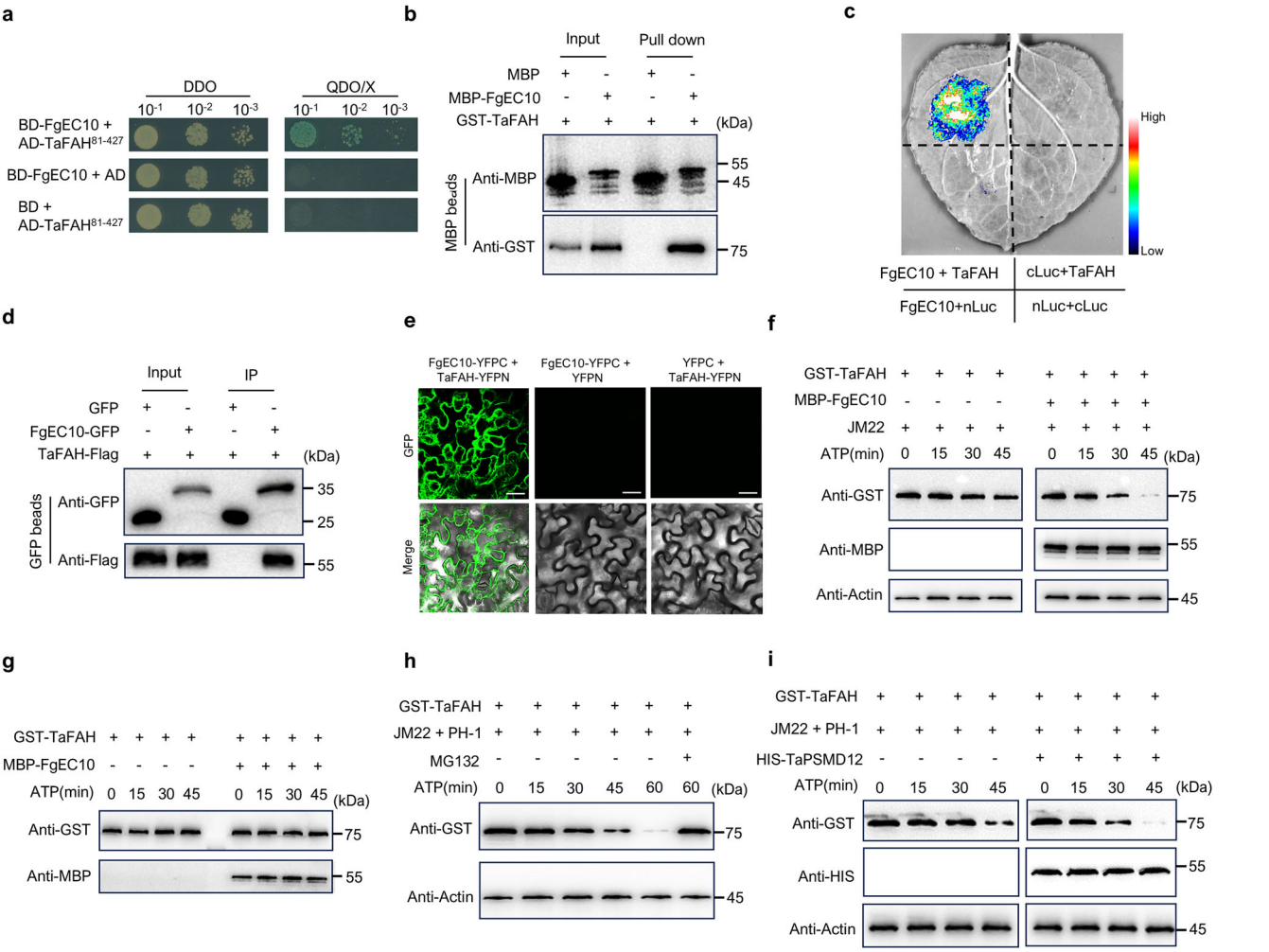

Fig. 3 | FgEC10 enhances the degradation of TaFAH mediated by the 26S proteasome system. a A yeast two-hybrid analysis of the interaction between FgEC10 and TaFAH$^{81-427}$. DDO, SD-Trp-Leu; QDO/X, SD-Trp-Leu-His-Ade containing X-α-gal. **b** In vitro pulldown assay to detect the interaction between FgEC10 and TaFAH. GST-TaFAH was pulled down by MBP-FgEC10 immobilized on MBP agarose beads but not by MBP. The input and pulldown proteins were detected with anti-GST and anti-MBP antibodies. **c** Luciferase complementation imaging assay to detect the interaction of FgEC10 with TaFAH in *N. benthamiana* leaves. FgEC10-cLuc and TaFAH-nLuc were co-expressed in *N. benthamiana* leaves by *A. tumefaciens*. The luminescence signal was observed at 72 hpi. **d** In vivo Co-IP detection of the interaction between FgEC10 and TaFAH. Total protein extracts were incubated with anti-GFP magnetic beads. The input proteins and precipitants were detected with anti-Flag and anti-GFP antibodies. **e** Interaction between FgEC10 and TaFAH was detected using BiFC assays. *N. benthamiana* leaves were infiltrated with a mixture of *A. tumefaciens* strains co-expressing indicated constructs. GFP signals were detected at 48 hpi. Bar, 20 μm. **f** Degradation of TaFAH was detected using a cell-free degradation assay. Mixtures containing 3.5 μg of recombinant GST-TaFAH, MBP-FgEC10, and 100 μL of total proteins extracted from wheat variety JiMai22 (JM22) were incubated for the indicated times. Western blot analysis was conducted using anti-MBP, anti-GST, and anti-Actin antibodies. **g** Mixtures containing equal amounts of MBP-FgEC10 and GST-TaFAH were incubated for the indicated times and detected with anti-MBP and anti-GST antibodies. **h** Degradation of TaFAH by total proteins in wheat heads inoculated with the WT strain was inhibited by the MG132 proteasome inhibitor. **i** Mixtures containing equal amounts of recombinant GST-TaFAH, HIS-TaPSMD12, and total proteins from wheat heads were inoculated with the WT strain and incubated for the indicated time. The mixtures were detected using anti-HIS, anti-GST, and anti-Actin antibodies.

(Fig. 3e). In contrast, no signal was detected when FgEC10-YFPC and TaFAH-YFPN were co-expressed with YFPN and YFPC control, respectively (Fig. 3e). The co-localization assay also showed that the distribution of FgEC10-GFP and TaFAH-mCherry in the plant cells was similar (Supplementary Fig. 10). Collectively, these findings demonstrate that FgEC10 interacts directly with TaFAH in plant cells. The wheat genome encodes three *TaFAH* paralogs: *TaFAH*, *TaFAH-B*, and *TaFAH-D* (Supplementary Fig. 11a). Protein interaction studies showed that FgEC10 can interact with TaFAH-B and TaFAH-D (Supplementary Fig. 11b, c). We compared the coding sequences of these three *TaFAH* homeoalleles and found that they shared 96.9% sequence identity and their encoded proteins were 96.2% identical, indicating functional redundancy between these three *TaFAH* paralogs (Supplementary Fig. 11).

FgEC10 promotes TaFAH degradation by the 26S proteasome system

A cell-free degradation assay was conducted to gain insight into the effect of FgEC10 on TaFAH in wheat. Equal amounts of GST-TaFAH recombinant proteins were co-incubated with total proteins extracted from the Fielder wheat head. GST-TaFAH was significantly degraded in the presence of MBP-FgEC10 recombinant protein. However, the TaFAH degradation rate was lower in the absence of MBP-FgEC10 (Fig. 3f). These results suggest that FgEC10 accelerates TaFAH degradation. However, TaFAH degradation was not detected in the co-incubation of GST-TaFAH and MBP-FgEC10, except when wheat head extract was added to the protein degradation assays (Fig. 3g). This finding demonstrates that specific components of wheat head extract are necessary for FgEC10-stimulated TaFAH degradation.

The ubiquitin-proteasome system is a conserved pathway for protein degradation[38]. To determine whether TaFAH degradation occurs through the ubiquitin-26S proteasome system, we first assayed the effect of the proteasomal inhibitor MG132 on TaFAH degradation. We observed an increase in TaFAH degradation over time in the presence of ATP; however, this effect was suppressed by MG132 (Fig. 3h). The PSMD regulatory subunit is a crucial component of the 26S proteasome[39]. Interestingly, we found that NtPSMD12 was identified from our previously FgEC10-GFP pulldown samples but not from the GFP pulldown samples (Supplementary Data 3). This led us to hypothesize that TaPSMD12 (the homolog of NtPSMD12) facilitates TaFAH degradation via the ubiquitin-26S proteasome pathway. We conducted in vitro degradation assays to examine the effects of TaPSMD12 on TaFAH and validate this hypothesis. After the addition of HIS-TaPSMD12 to the mixture of GST-TaFAH and total protein extracted from wheat heads, the band of recombinant GST-TaFAH proteins in the western blot detection exhibited weaker signals over time than those observed in the absence of HIS-TaPSMD12 (Fig. 3i). Additional ubiquitination assay indicated that FgEC10 and TaPSMD12 did not promote TaFAH ubiquitination (Supplementary Fig. 12). These results revealed that the 26S proteasome degrades TaFAH, but not via TaFAH ubiquitination.

FgEC10 promotes the interaction of TaFAH and TaPSMD12

We conducted an in vitro pulldown assay to test whether TaFAH directly interacted with TaPSMD12. HIS-TaPSMD12 was pulled down with GST-TaFAH, but not with the control GST protein (Fig. 4a). LCI assays showed that the co-expression of TaFAH-nLuc and TaPSMD12-cLuc resulted in robust luciferase signals in *N. benthamiana* leaves (Fig. 4b). The interaction between TaFAH and TaPSMD12 in plants was also confirmed using co-IP assays (Fig. 4c). Additional co-expression of TaFAH-GFP and TPSMD12-mCherry showed the co-localized fluorescent signal (Supplementary Fig. 13). Collectively, these findings suggest that TaFAH interacts with TaPSMD12 both in vitro and in vivo.

To better understand the relationship among FgEC10, TaFAH, and TaPSMD12, we conducted experiments to determine whether FgEC10 affects the strength of the TaFAH-TaPSMD12 interaction. When TaFAH, TaPSMD12, and FgEC10 were co-expressed in yeast cells, colonies developed quickly on SD-Leu-Trp-His-Met plates (Fig. 4d). However, suppressing the expression of FgEC10 in the SD-Leu-Trp-His medium resulted in a weaker interaction between TaFAH and TaPSMD12 (Fig. 4d; Supplementary Fig. 14). We conducted a pulldown assay using recombinant HIS-TaPSMD12, TaFAH-GST, and MBP-FgEC10 proteins. When equal amounts of HIS-TaPSMD12 and TaFAH-GST were co-incubated with GST beads, the gradual addition of increasing concentrations of FgEC10 resulted in a concentration-dependent increase in the amount of TaPSMD12 copurified with TaFAH-GST (Fig. 4e). We conducted an LCI assay to confirm this enhancement effect *in planta*. The expression of FgEC10 resulted in an increase in the fluorescence signals of luciferase recovered by TaFAH-nLuc and TaPSMD12-cLuc compared to the luciferase signals without FgEC10 (Fig. 4f). Quantification analysis further indicated that the catalytic activity of luciferase in leaves expressing FgEC10 increased by 41.6% compared to that in leaves without FgEC10 (Fig. 4g). These findings suggest that FgEC10 promotes interactions between TaFAH and TaPSMD12.

TaFAH positively regulates wheat resistance against *F. graminearum*

We analyzed *TaFAH* transcript levels during *F. graminearum* infection of wheat heads at different time points post-inoculation. *TaFAH* was rapidly up-regulated after *F. graminearum* infection and then decreased to normal levels (Supplementary Fig. 15).

TaFAH was overexpressed in the wheat cultivar Fielder to investigate the role of *TaFAH* in resistance against *F. graminearum* (Supplementary Fig. 16a). Eight transgenic plants were identified from ten T0 plants (Supplementary Fig. 16b). The expression level of *TaFAH* was up-regulated 5–8 fold in T0-*TaFAH*-OE-1, -3, and -4 plants compared to that in the control Fielder plants (Supplementary Fig. 16c). Furthermore, T1 generation plants derived from these three positive T0 generation plants were verified (Supplementary Fig. 16d, e). Transgenic wheat plants overexpressing *TaFAH* showed increased resistance to *F. graminearum* in wheat head infection experiments (Fig. 5a). In comparison to Fielder plants, the disease index, fungal biomass, and DON content were reduced significantly in *TaFAH*-overexpressing plants, respectively (Fig. 5b–d).

We also generated *TaFAH*-RNAi transgenic plants (Supplementary Fig. 17a). Ten positive transgenic plants were screened from the T0 plants (Supplementary Fig. 17b). We identified T0-*TaFAH*-RNAi-1, -2, -5, and -6 plants in which the expression level of *TaFAH* was reduced by approximately 90% compared to that of the control Fielder plants (Supplementary Fig. 17c). Furthermore, *TaFAH*-RNAi fragment and the *TaFAH, TaFAH-B, and TaFAH-D* expression in the leaves were confirmed in three T1 generation plants (Supplementary Fig. 17d, e). When inoculated with the WT strain, *TaFAH*-RNAi T1 plants displayed more severe FHB symptoms than Fielder plants (Fig. 5a) and had a higher disease index, fungal biomass, and DON content (Fig. 5b–d). Collectively, these results revealed that TaFAH can increase wheat resistance to *F. graminearum*.

Overexpression of *TaFAH* promotes wheat heading

We assessed the agronomic characteristics of transgenic plants to examine the effect of *TaFAH* on wheat growth. We found that the heading dates of *TaFAH*-overexpressing plants were approximately 10 days earlier than those of control plants (Fig. 6a, e). Thousand-grain weight, grain width, and length increased slightly but not significantly in *TaFAH*-overexpressing plants compared to control plants (Fig. 6c, e). No differences were observed between *TaFAH*-overexpressing plants and control Fielder plants with regard to plant height, panicle number per plant, spike length, and grain number per spike (Fig. 6b–e). For RNAi plants, there was no difference in agronomic characteristics compared to the control (Fig. 6). Collectively, these results suggest that excessive expression of *TaFAH* in wheat shortens the heading period.

TaFAH promotes the expression of genes that are associated with disease resistance and plant heading

We performed RNA-seq analysis to investigate the genes associated with FHB resistance and heading dates in *TaFAH* transgenic plants. A total of 2112 differentially expressed genes (DEGs) were found in *TaFAH*-OE plants compared to *TaFAH*-RNAi plants. Of these, 1635 DEGs were up-regulated in *TaFAH*-OE plants (Fig. 7a and Supplementary Data 4). Gene Ontology (GO) enrichment analysis indicated that ATP binding, protein kinase, protein phosphorylation, DNA-binding transcription factors, regulation of DNA-templated transcription, calcium ion binding, response to stimulus, and ethylene-activated signaling pathways were enriched (Fig. 7b). Kyoto Encyclopedia of Genes and Genomes (KEGG) pathway enrichment analysis indicated that the overproduction of TaFAH notably stimulated plant immunity pathways, such as the mitogen-activated protein kinase (MAPK) signaling pathway, plant hormone signal transduction, and plant-pathogen interaction (Fig. 7c). In addition, 5 MAPKs, 36 nucleotide-binding domain and leucine-rich repeat (NBS-LRR) proteins responsible for disease resistance, 7 chitinases, and 5 respiratory burst oxidase homologs (RBOHs) encoding genes were up-regulated in *TaFAH*-OE plants compared to *TaFAH*-RNAi plants (Fig. 7d). These genes play roles in plant immunity against microbial pathogens[40–42]. We also found that the expression of six *Flowering locus T* genes was up-regulated in *TaFAH*-overexpressing plants compared to *TaFAH*-RNAi (Fig. 7d). This was consistent with the earlier-heading phenotype of

https://doi.org/10.1038/s41467-025-60736-y

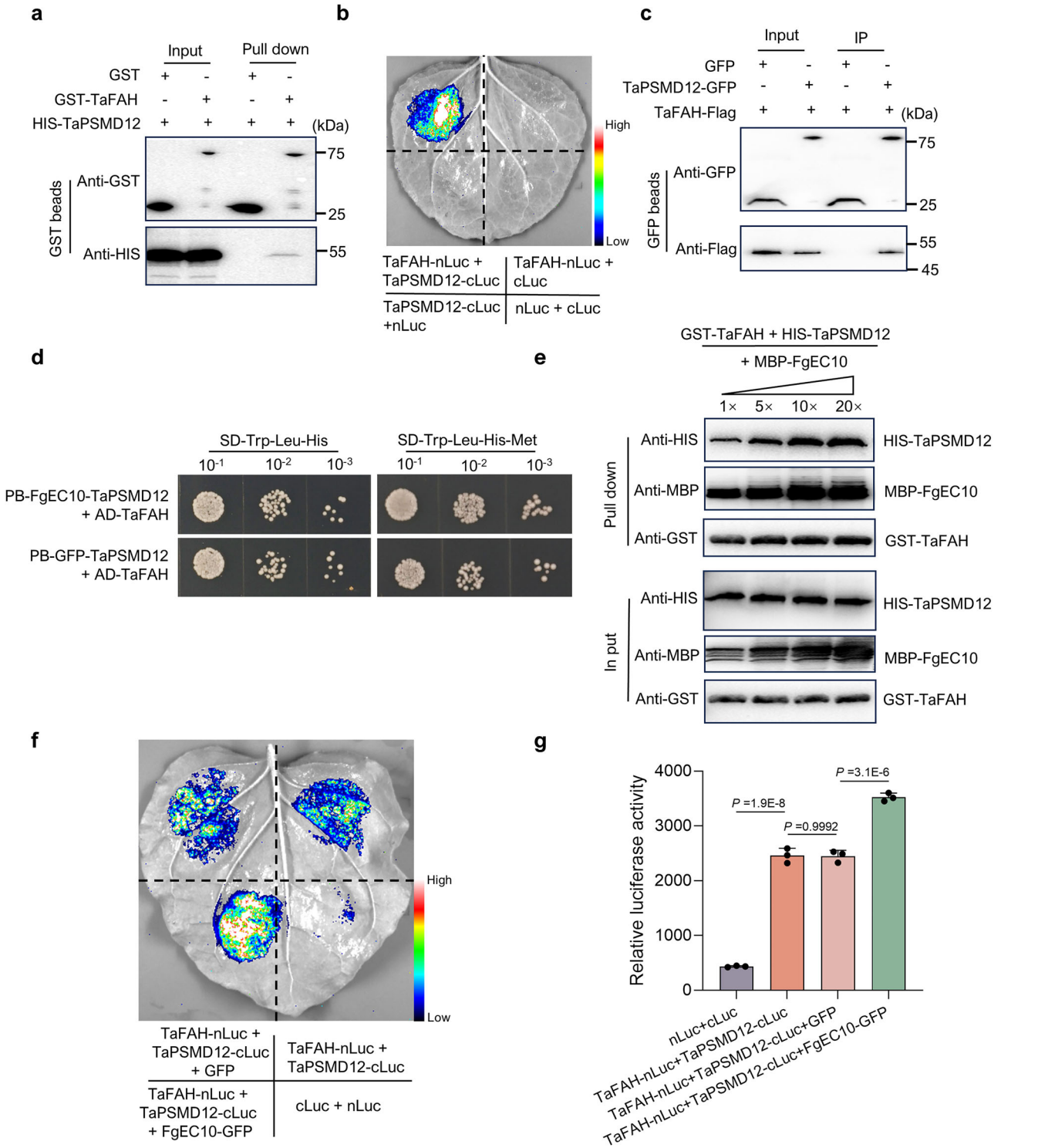

Fig. 4 | FgEC10 promotes the interaction between TaFAH and TaPSMD12. a GST pulldown assay to detect the interaction between TaPSMD12 and TaFAH. HIS-PSMD12 was pulled down by GST-TaFAH immobilized on GST agarose beads but not by GST. The input and pulldown proteins were detected with anti-GST and anti-HIS antibodies. **b** Luciferase complementation imaging assay to investigate the interaction between TaFAH and TaPSMD12. TaPSMD12-cLuc and TaFAH-nLuc were co-expressed in *N. benthamiana* leaves by *A. tumefaciens*. The luminescence signal was observed at 72 hpi. **c** Co-IP assays to detect the interaction between TaFAH and TaPSMD12. Total protein extracted from *N. benthamiana* leaves was incubated with anti-GFP magnetic beads. The input proteins and precipitants were detected with anti-Flag and anti-GFP antibodies. **d** Yeast tri-hybrid analysis of the interaction between TaFAH and TaPSMD12 in the presence or absence of FgEC10. The expression of *FgEC10* was suppressed in the presence of methionine (SD-Trp-Leu-His medium) and induced in the absence of methionine (SD-Trp-Leu-His-Met medium). GFP replaced FgEC10 was used as a control. **e** Pulldown assay to investigate the impact of FgEC10 on the interaction between TaFAH and TaPSMD12. GST-TaFAH and HIS-TaPSMD12 were incubated with increasing amounts of MBP-FgEC10. The mixtures were pulled down by GST-TaFAH immobilized on GST agarose beads and then analyzed with anti-GST, anti-MBP, and anti-HIS antibodies. The assay was repeated twice with similar results. **f** LCI assay to examine the interaction between TaFAH and TaPSMD12 in co-expression with FgEC10. **g** Quantification of luciferase activity in the leaves shown in (**f**). Bars represent mean ± SD from three independent replicates (one-tailed Student's *t*-test).

https://doi.org/10.1038/s41467-025-60736-y

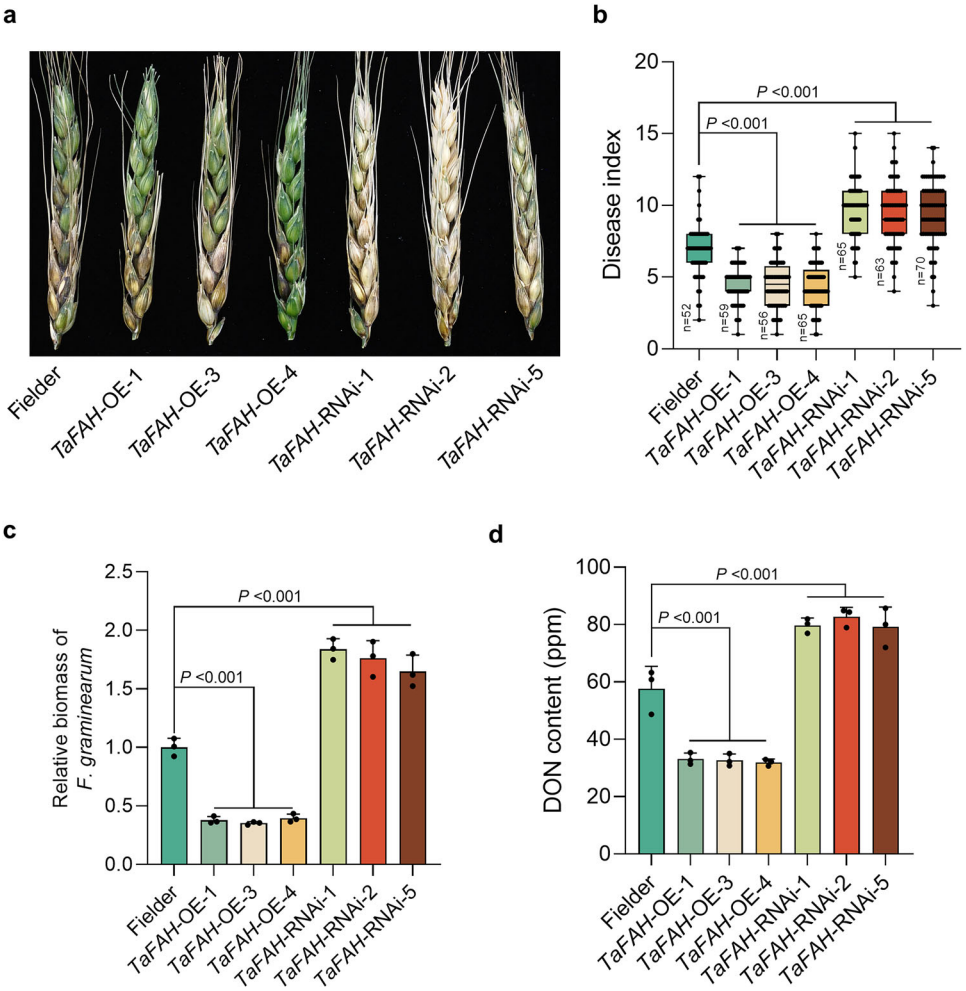

Fig. 5 | TaFAH positively regulates wheat resistance to *F. graminearum*. **a** Wheat heads of the cultivar Fielder overexpressing or silencing *TaFAH* were inoculated with the WT strain, and photos were taken at 14 dpi. **b** The disease index was determined through three independent trials. In the box plots: center line, median; box, interquartile range; whiskers, 1.5× interquartile range; and point, the disease index for each head. **c** Fungal biomass assayed by qPCR with DNA isolated from the same set of wheat heads as in (**b**). **d** DON levels were quantified in the indicated wheat spikelets. All the data were calculated from three independent replicates and presented as means ± SD (one-way ANOVA test between Fielder and transgenics).

TaFAH-overexpressing plants. Moreover, the transcript levels of a vast number of transcription factor genes increased, including 42 WRKY transcription factors, 40 ethylene-responsive transcription factors, 23 bHLH DNA-binding proteins, 15 NAC transcription factors, and 28 MYB transcription factors (Fig. 7d). Our transcriptomic analysis revealed that TaFAH plays an important role in various biological processes relevant to wheat heading and pathogen defense.

TaFAH increases the contents of amino acids associated with FHB resistance

FAH is an enzyme catalyzing fumarylacetoacetate (FAA) into fumarate and acetoacetate[43]. To test the biochemical properties of TaFAH, we overexpressed TaFAH in the tobacco leaves and determined the product of acetoacetate content. The results showed that the tobacco leaves overexpressing TaFAH produced more acetoacetate than the GFP control, indicating that TaFAH has the fumarylacetoacetate hydrolase activity (Supplementary Fig. 18). To test whether FgEC10 influences the enzyme activity of TaFAH, we overexpressed FgEC10 and TaFAH in the tobacco leaves, and the results showed that tobacco leaves overexpressing both FgEC10 and TaFAH produced similar levels of acetoacetate compared to tobacco leaves overexpressing only TaFAH, suggesting that FgEC10 has no effect on the enzyme activity of TaFAH (Supplementary Fig. 18).

The metabolic products of FAA enter the tricarboxylic acid (TCA) cycle[44]. A metabolomic analysis of wheat was carried out during the flowering stage to determine the effect of *TaFAH* overexpression on metabolites. We identified 445 differential metabolites, including 168 up-regulated and 277 downregulated metabolites, in *TaFAH*-overexpressing plants compared to *TaFAH*-RNAi plants (Supplementary Fig. 19a and Supplementary Data 5). The differential metabolites were classified into ten categories: 9.28% amino acids, peptides, and analogs; 6.84% carbohydrates and carbohydrate conjugates; 1.38% benzoic acids and derivatives; 1.77% carbonyl compounds; 1.44% eicosanoids; 4% fatty acids and conjugates; 1.43% fatty acyl glycosides; 3.58% flavonoid glycosides; 1.25% terpene glycosides; and 69.03% others (Fig. 8a). KEGG analysis demonstrated that the up-regulated metabolites were enriched in several metabolic processes, including translation, nucleotide metabolism, terpenoid and polyketide metabolism, cofactor and vitamin metabolism, membrane transport, lipid metabolism, carbohydrate metabolism, and amino acid metabolism (Supplementary Fig. 19b). Notably, amino acids exhibited the most significant differences among the up-regulated metabolites (Fig. 8a, b).

To validate the untargeted metabolome data, we performed a targeted metabolome to determine the levels of amino acids. The results confirmed that the levels of several amino acids are up-

https://doi.org/10.1038/s41467-025-60736-y

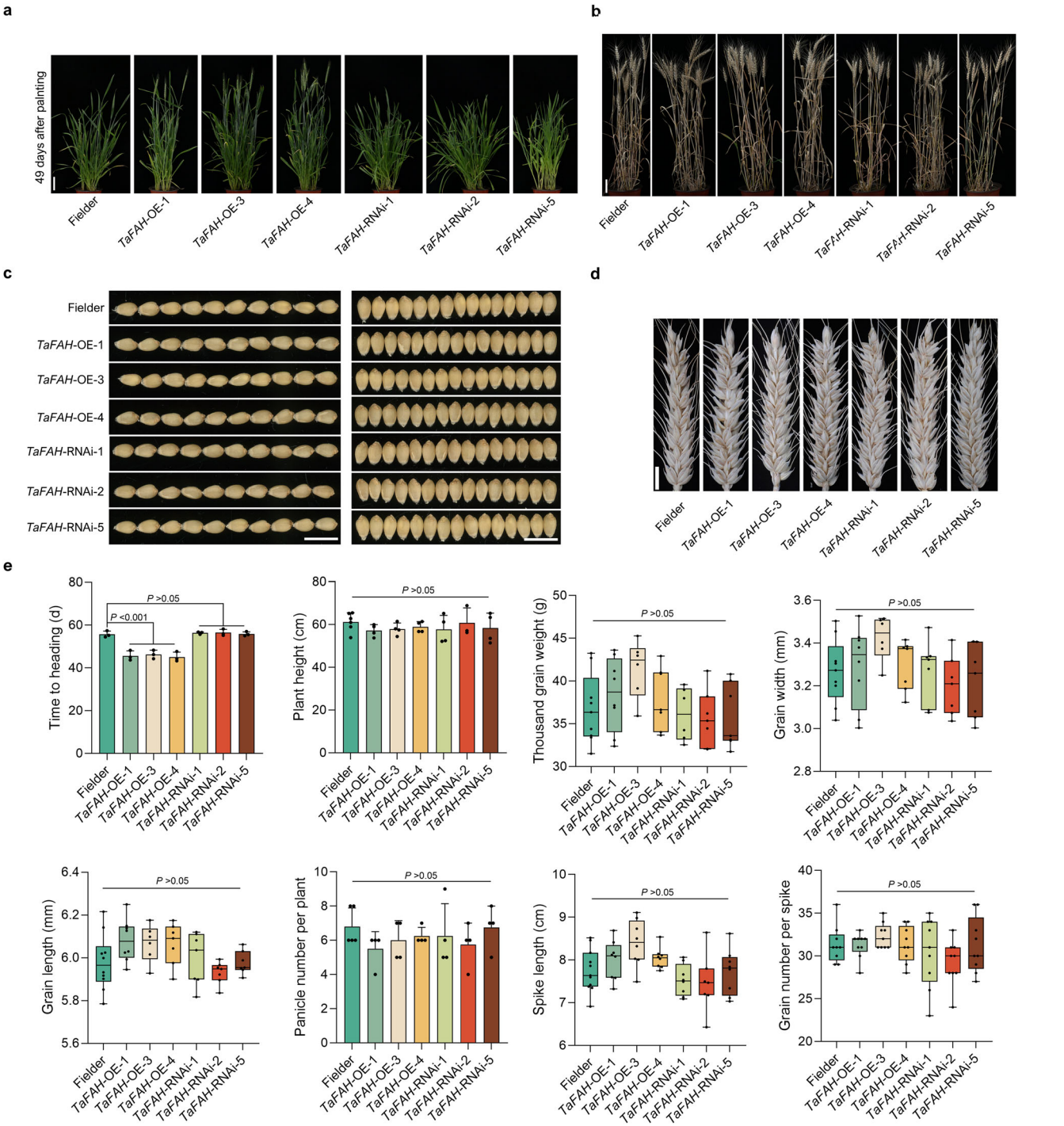

Fig. 6 | Agronomic traits of Fielder, *TaFAH*-OE, and *TaFAH*-RNAi plants. **a** Images of Fielder, *TaFAH*-OE, and *TaFAH*-RNAi plants 42 days after planting. Bar, 10 cm. **b** Mature plants of Fielder, *TaFAH*-OE, and *TaFAH*-RNAi plants. Bar, 10 cm. **c** Seed shape of Fielder, *TaFAH*-OE, and *TaFAH*-RNAi plants at the kernel ripe stage. Bar, 1 cm. **d** Spike phenotypes of Fielder, *TaFAH*-OE, and *TaFAH*-RNAi plants at the kernel ripe stage. Bar, 1 cm. **e** Time to heading, plant height, panicle number per plant, spike length, grain number per spike, grain width, grain length, and thousand-grain weight of Fielder, *TaFAH*-OE, and *TaFAH*-RNAi plants. Values represent the means ± SD from at least three independent replicates. All the data were compared to that of wild-type Fielder using a one-way ANOVA test. In the box plots: center line, median; box, interquartile range; whiskers, 1.5× interquartile range; and point, the data for agronomic traits.

regulated in *TaFAH*-overexpressing plants compared to *TaFAH*-RNAi plants (Supplementary Fig. 19c; Supplementary Data 6). We then examined the impact of seven up-regulated amino acids on hyphal growth and found that lysine (Lys) inhibited the growth of *F. graminearum* (Supplementary Fig. 20). Furthermore, exogenous application of His, Lys, and Ser improved wheat head and seedling resistance to *F. graminearum* (Fig. 8c–e; Supplementary Fig. 21).

Discussion

When attacked by harmful pathogens, plants use pattern-recognition receptors that recognize pathogen-associated molecules to stimulatepattern-triggered immunity (PTI)[45]. Phytopathogens secrete numerous effector proteins that perturb plant key immune or metabolic processes to counter this defense[14,46]. *F. graminearum* secretes many proteins during wheat infection; however, its

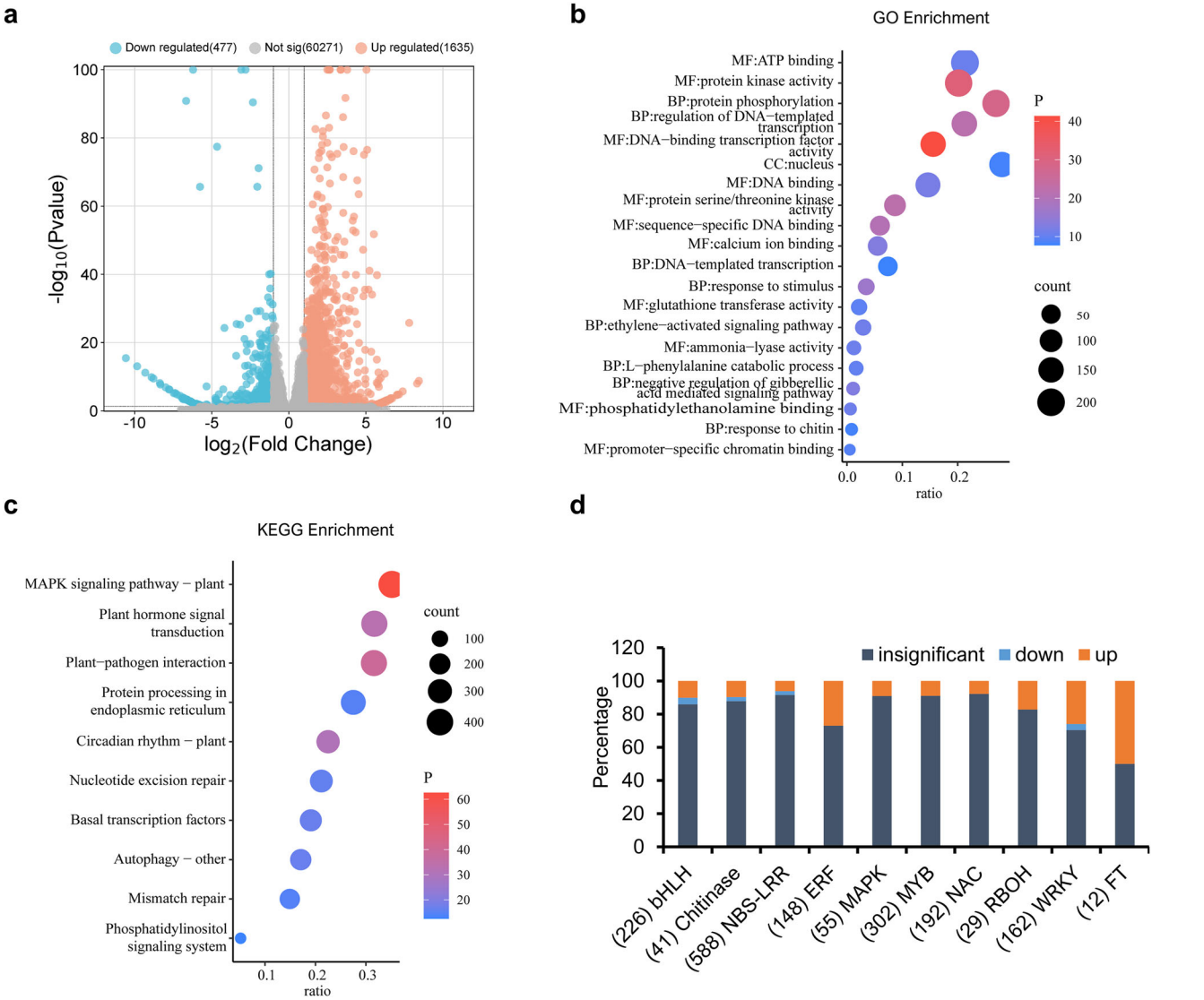

Fig. 7 | TaFAH regulates a subset of gene expression. a Volcano plot showing the differential expression of genes in the *TaFAH*-OE and *TaFAH*-RNAi plants. Thresholds of significantly ($P < 0.05$) downregulated (blue dots, $\log_2$ (fold change) < −1) and up-regulated expression (light pink dots, $\log_2$ (fold change) > 1) are highlighted. **b**, **c** GO and KEGG enrichment analysis of the up-regulated genes in (**a**). **d** Stacked bar chart shows the expression of disease-resistance-related genes, transcription factors, and flowering-related genes in *TaFAH*-OE in comparison with those in *TaFAH*-RNAi. P: Probability of random enrichment. Ratio: Proportion of differentially expressed genes (DEGs) in the pathway relative to its total gene count. Count: gene count.

virulence mechanisms are largely unknown. In the present study, we demonstrated that *F. graminearum* delivers a virulent cytoplasmic effector, FgEC10, to target the host TaFAH protein. FgEC10 facilitates the interaction between TaFAH and TaPSMD12 and promotes TaFAH degradation via the 26S protease system. TaFAH positively regulated wheat FHB resistance by inducing resistance gene expression and increasing amino acid content (Fig. 8f). Understanding the molecular mechanisms underlying the virulence of *F. graminearum* effectors is crucial for developing effective disease management strategies and molecular breeding.

The 26S proteasome plays a major role in selective protein degradation in eukaryotic cells. The components and subunit interaction maps are conserved in plant and yeast for the 19S regulatory subcomplex of the proteasome, which is responsible for substrate specificity[47]. In *Arabidopsis*, Regulatory Particle non-ATPase 5 (RPN5), the homolog of human PSMD12, which is a subunit of the 19S regulatory subcomplex, plays important roles in gametogenesis, sporophyte development[48]. In the present study, TaFAH degradation was accelerated by the 26S proteasome regulatory subunit TaPSMD12, and TaFAH destabilization was restored by the proteasome inhibitor MG132, revealing that TaFAH degradation is 26S proteasome-dependent. Furthermore, our findings reveal a degradation mechanism in which the *F. graminearum* effector FgEC10 promotes the proteasomal degradation of target proteins by enhancing the interaction between the target protein and the 26S proteasome regulatory subunit. Future studies investigating whether FgEC10 can target other wheat proteins and interfere with their functions will contribute to a comprehensive understanding of FgEC10's pathogenic mechanisms.

In *Arabidopsis*, the *FAH* mutation caused cell death phenotypes under short-day conditions (Han et al. [43]). FAH catalyzes the final step in tyrosine degradation in animals and plants, which cleaves fumarylacetoacetate into acetoacetate and fumarate, which feed into the TCA cycle[43,44]. The TCA cycle provides the essential precursors for respiration, amino acid biosynthesis, and nitrogen metabolism[49]. In this study, the overexpression of *TaFAH* significantly increased the accumulation of various amino acids, according to metabolomic analysis. Previous research has shown that the treatment of rice with exogenous amino acids triggers systemic immunity, such as

https://doi.org/10.1038/s41467-025-60736-y

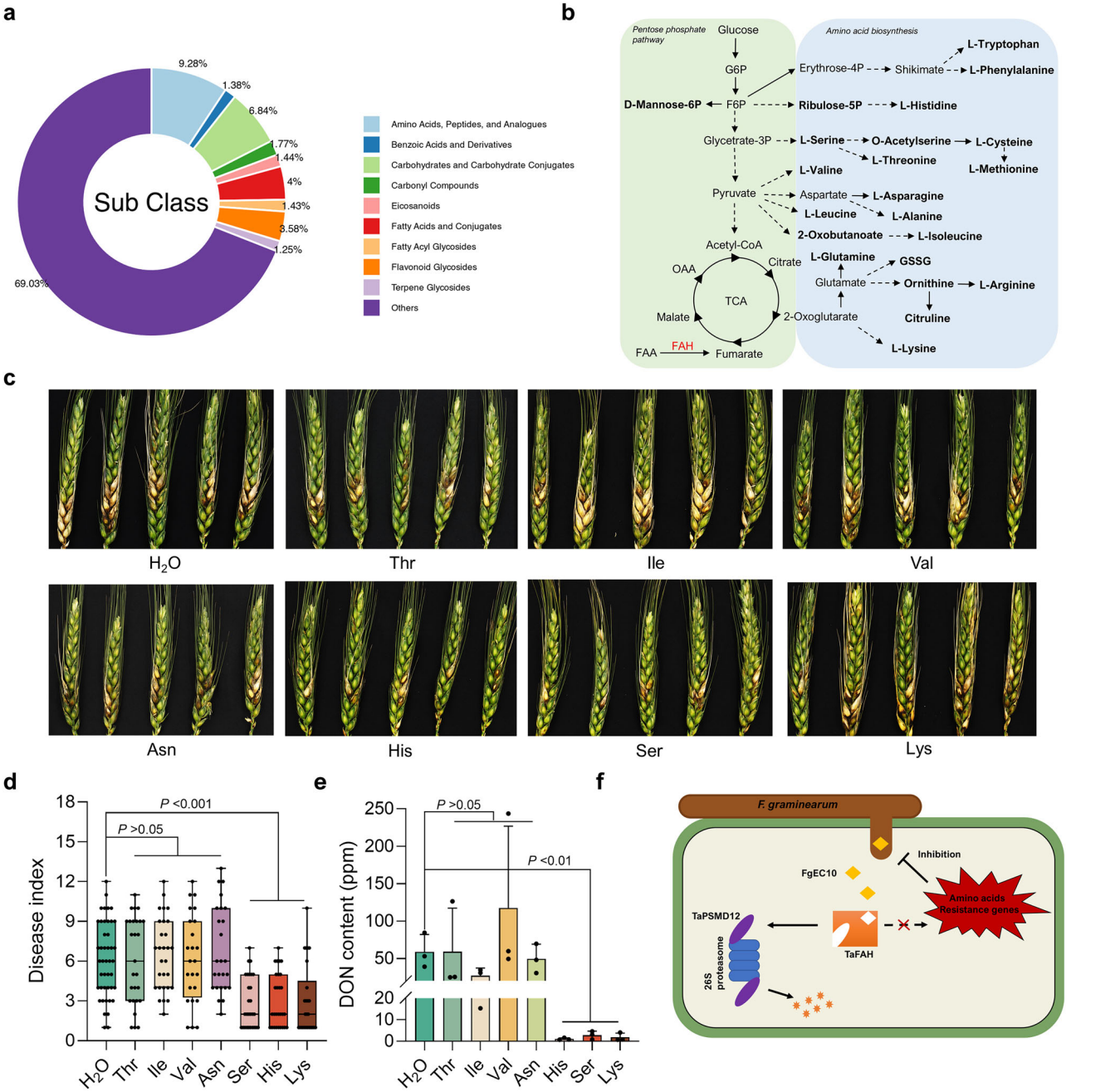

Fig. 8 | TaFAH regulates a subset of amino acid contents with antifungal activity. a Pie chart representing the subclassification of differential metabolites (Fold change > 1.2, VIP > 1, and $P < 0.05$) in untargeted metabolome analysis. **b** Schematic diagram of TCA and amino acid metabolic pathways. Bold letters represent the up-regulated metabolites in targeted or untargeted metabolome analysis. **c** The FHB symptoms of spikelets sprayed with the indicated amino acid solution. His, Ser, and Lys treatments can significantly reduce the number of diseased spikelets. Symptoms were photographed at 10 dpi. **d** The disease indexes in (**c**). **e** The DON levels in diseased wheat spikelets in (**c**). In (**d**) and (**e**), data are presented as mean ± SD from three independent replicates. All the data were compared to that of H_2O treatment using a one-tailed Student's *t*-test. **f** Working model showing the molecular mechanism of FgEC10 in the suppression of wheat immunity. During infection, *F. graminearum* releases effector FgEC10 from its infectious hyphae into plant cells. FgEC10 specifically targets TaFAH, which positively regulates resistance to *F. graminearum* in wheat. TaFAH can be degraded by the 26S proteasome through its association with the 26S proteasome regulatory subunit TaPSMD12 in plant cells. By promoting the interaction of TaFAH with TaPSMD12, FgEC10 enhances the degradation of TaFAH by the 26S proteasome, reducing amino acid contents and resistance gene expressions, thereby compromising the ability of wheat to counteract *F. graminearum* infection.

glutamate-induced resistance in rice[50]. Amino acid fertilizers can improve crop yield and quality by recruiting beneficial rhizosphere microbes[51]. In addition, exogenous amino acids and *F. graminearum* inoculation assays showed that Pro and Ala increased wheat resistance to FHB[52]. Our study showed that Lys exhibited inhibitory activity against *F. graminearum*, and exogenous application of His, Lys, and Ser significantly increased wheat head and seedling resistance to *F. graminearum*. RNA-seq results indicated that TaFAH activates the expression of several defense-related genes implicated in MAPK, NBS-LRR, chitinase, oxygen-producing proteins (RBOHs), and disease-resistance proteins. These genes were enriched among the up-regulated DEGs in plants overexpressing *TaFAH*. MAPK and WRKY transmit biotic stress signals from membrane receptors to the nucleus, thereby activating downstream responses to pathogens[53,54].

Chitinases degrade fungal cell walls and restrict the spread of pathogens in plant tissues[42]. Activation of plant respiratory burst oxidase homologs (RBOHs) for the production of reactive oxygen species (ROS) is a significant event in defense signaling, and ROS are also toxic to fungal hyphae[41]. Overall, our results indicate that TaFAH increases the resistance of wheat to *F. graminearum* by increasing the content of specific amino acids and activating the expression of disease-resistant genes.

Achieving a balance among plant growth, yield, and disease resistance is challenging. Plant growth and development principally depend on several immunity-associated pathways, including hormonal regulation, energy and secondary metabolism, gene transcriptional reprogramming, and signal transduction. Modifying essential genes within these pathways frequently affects plant growth and development[12]. MPK4, a HopAI1 effector target, negatively affects the salicylic acid response in *Arabidopsis thaliana*. Its loss leads to dwarfism and spontaneous lesions while improving resistance against *Pseudomonas syringae* and the oomycete *Peronospora parasitica*[55,56]. Additionally, the *M. oryzae* effector Avr-Pita binds to rice Pita and is associated with decreased seed weight[57]. Mutations in SPL28 increase resistance to *M. oryzae* but reduce grain quality and yield[58]. In this study, we showed that the overexpression of *TaFAH* increased resistance to *F. graminearum* and shortened heading time in wheat.

Efficient identification of disease resistance or disease susceptibility genes guided by effector proteins is an effective approach for improving plant resistance breeding. For example, the PhRXLRC01 effector from *Plasmopara halstedii* has led to the identification of a broad-spectrum resistance gene (PI22) in sunflowers[59]. Knocking out the wheat susceptibility gene *TaPsIPK1*, which is targeted by the fungal effector PsSpg1, provides broad-spectrum resistance against the *Pst* pathogen without affecting wheat agronomic traits[33]. *U. virens* secretes UvCBP1, a cytoplasmic effector that interacts with the rice scaffold protein OsRACK1A to facilitate infection of rice flowers. Overproduction of OsRACK1A confers rice floral resistance to *U. virens*[34]. Bread wheat is an allohexaploid crop in which most genes have six similar copies, with functional redundancy in A, B, and D subgenomes[31]. The complex genome makes it difficult to identify FHB resistance genes. By studying the pathogenic mechanism of the *F. graminearum* effector protein FgEC10, we identified an important FHB resistance gene, *TaFAH*. Our study offers a valuable gene resource for achieving an equilibrium between disease resistance and crop performance. Gene editing can be used to modify the promoter region to enhance *TaFAH* expression, thereby improving disease resistance. In addition, His, Ser, and Lys have the potential to be used as green pesticides to reduce FHB incidence and mycotoxin accumulation in cereals.

Methods

Growth conditions of plant materials and fungal strains

The wheat cultivar Fielder and JiMai 22 (JM22) were cultured in a greenhouse at 22 °C with a light/dark cycle of 16/8 h or grown on an agricultural experimental farm in Shenzhen, Guangdong Province, China, for pathogen inoculation assays. The heading date of each wheat plant was determined as the number of days from sowing to the stage when 50% of the spikes had fully emerged. *N. benthamiana* was grown in a growth chamber at 21–23 °C under a 14-h light and 10-h dark photoperiod. The *F. graminearum* PH-1 wild-type and mutant isolates were grown in the dark at 25 °C on potato dextrose agar (PDA) medium.

F. graminearum transformation

The protoplasts were generated through the incubation of young *F. graminearum* hyphae produced by conidia in yeast extract peptone dextrose (YEPD) medium with an enzymatic lysis buffer (25 g L^{-1} driselase and 5 g L^{-1} lysing enzyme in 1.2 M KCl) for 2–3 h at 28 °C. The lytic product was filtered through Miracloth, and protoplasts were harvested in STC buffer (200 g L^{-1} sucrose, 0.5 M Tris-Cl, pH 8.0, 0.05 M $CaCl_2$) at a concentration of 10^5 cells/mL. We employed a split-marker disruption system to generate Δ*FgEC10* mutants[60]. The strategy for deleting *FgEC10* is illustrated in Supplementary Fig. 1c. First, the 5′ and 3′ flanking sequences of *FgEC10* were amplified from genomic DNA by polymerase chain reaction (PCR) with FgEC10LF/FgEC10LR and FgEC10RF/FgEC10RR primers, respectively. The resulting amplicons were then fused with the 5′ and 3′ fragments of the hygromycin phosphotransferase cassette (*hph*) using double-jointed PCR. Next, we amplified the overlapping fragments with FgEC10LFNest/HYRNest and NYGFNest/FgEC10RRNest primers. The fusion PCR product was transformed into *F. graminearum* protoplasts using a PEG-mediated transformation method[9]. The 1.9-kb region containing *FgEC10* and its promoter was ligated into the pHZ100 vector and transformed into Δ*FgEC10*-12 mutant protoplasts for the complementation assay. The primers used in this study are listed in Supplementary Data 7.

Infection assays

Conidia were collected from the carboxymethyl cellulose (CMC) medium and reached 10^5 spores/mL in sterile distilled water. A 10 μL conidium suspension was injected into the fourth or fifth spikelet from the base of flowering wheat heads of cultivars JiMai 22 or Fielder. The inoculated wheat heads were incubated in bags at high humidity for 48 h. The number of infected spikelets in each wheat head was recorded as the disease index 14 days after inoculation. Simultaneously, the whole wheat head was sampled to measure DON production using the DON Quantification Kit Wis008 (Wise Science, Zhenjiang, China), according to the manufacturer's instructions. The DON production by *F. graminearum* hyphae was determined in our previous study[37].

Histological observation

N. benthamiana leaves expressing *FgEC10* were sprayed with 20 μM flg22 or 1 μM chitin, decolorized in destaining solution (alcohol: acetic acid, 1:1 v/v), and stained with 0.05% aniline blue in phosphate buffer (pH 9.5) to determine the papillary callose accumulation. For scanning electron microscope (SEM) analysis, the inoculated lemmas were sampled at 48 hpi and were fixed in 4% glutaraldehyde for 48 h at 4 °C. The specimens were dehydrated in a graded series of ethanol for 10 min each, dried with a critical point dryer, affixed to aluminum stubs, and conductively coated with gold/palladium. The coated samples were observed under a JSM 6360LV SEM (JEOL Ltd., Tokyo, Japan) at 15 KV.

ROS accumulation detection

Plugs (6 mm diameter) were punched from *N. benthamiana* leaves expressing FgEC10 and incubated in water in a 96-well plate to examine the ROS burst. After 18 h, 200 μL of luminescence detection buffer (20 μM flg22 or 1 μM chitin, 100 mM luminol, and 20 mg/mL horseradish peroxidase) was added to plates, and the luminescence was recorded by a microplate reader for 55 min. The data from eight biologically independent samples were recorded.

RNA extraction and RT-qPCR assays

Total wheat flowering head RNA was extracted using the MiniBEST Plant RNA Extraction Kit (Takara, Dalian, China) following the manufacturer's instructions. First-strand complementary DNA (cDNA) was synthesized using a PrimeScript1st Strand cDNA Synthesis Kit (Takara, Dalian, China) according to the manufacturer's protocol. RT-qPCR was performed using an Applied Biosystems StepOnePlus Real-Time PCR System with ChamQ Universal SYBR qPCR Master Mix according to the manufacturer's instructions to determine the expression of the selected genes and confirm the overexpression or silencing of transgenic wheat. *FgActin* or *TaActin* was used as an endogenous reference gene,

and the data were analyzed using the comparative $2^{-\Delta\Delta Ct}$ method. Each experiment included three independent biological replicates.

Yeast two-hybrid and tri-hybrid assays

Total RNA was extracted from the wheat flowering heads of JiMai 22 inoculated with PH-1 at 0, 24, 48, and 72 hpi to construct the yeast two-hybrid library. The FgEC10$^{\Delta SP}$ coding sequence was cloned into the pGBKT7 vector for library screening. The constructed pGBKT7-FgEC10$^{\Delta SP}$ was co-transformed with library plasmids into the Y2HGold yeast strain. Yeast colonies grown on SD-Trp-Leu-His-Ade containing x-α-gal were isolated as the putative targets.

The CDSs of targets were cloned into pGADT7 and then transformed in pairs into the yeast strain Y2HGold for point-to-point verification of interactions between FgEC10$^{\Delta SP}$ and candidate targets. The relevant plasmid combinations were introduced into yeast cells, and transformants were selected on synthetic drop-out (SD) medium devoid of Trp and Leu. Transformants were transferred to a medium devoid of Trp, Leu, His, and Ade to investigate growth.

The FgEC10$^{\Delta SP}$ and TaPSMD12 were ligated into the pBridge vector to perform the yeast three-hybrid assays. The pGADT7-TaFAH and pBridge-FgEC10$^{\Delta SP}$-TaPSMD12 constructs were transformed into the Y2HGold yeast strain. The transformants were grown on SD-His-Leu-Trp or SD-His-Leu-Trp-Met plates.

Secretion assay and confocal observation

The coding sequence of *FgEC10* was fused to the TrpC promoter and cloned into a pHZ100 vector for the secretion assay. The resulting construct was transformed into the wild-type strain PH-1. The strains were cultured in liquid medium for 3 days, and the fungal tissue and culture filtrate were isolated by centrifugation at 8000 × *g* for 10 min to detect effector secretion. The supernatants were added to 20% TCA after filtration through 0.22-μm-diameter filters and incubated at 4 °C overnight to obtain protein precipitates. The samples were then centrifuged for 10 min at 15,000 × *g* at 4 °C. Protein precipitates were washed three times with cold acetone and dissolved in a solution containing 8 M Urea, 100 mM Tris-HCl (pH 8.0), and 1× protease inhibitor cocktail (Roche). The samples were stored at −80 °C for immunoblotting. Agar disks containing hyphae expressing FgEC10-GFP were used to inoculate wheat coleoptiles to determine the localization of FgEC10 during plant infection. GFP signals in plant tissues were examined at 2 dpi using a confocal imaging microscope at excitation and emission wavelengths of 488 nm/507 nm.

Luciferase complementation imaging (LCI) assay

The coding sequences of *FgEC10*$^{\Delta SP}$ and *TaPSMD12* were cloned into the pCambia1300-cLuc vector to construct FgEC10$^{\Delta SP}$-cLuc and TaPSMD12-cLuc, respectively. Similarly, the TaFAH sequence was fused to the pCambia1300-nLuc vector to generate TaFAH-nLuc. These constructs were transformed into the *A. tumefaciens* strain GV3101 and co-agroinfiltrated into *N. benthamiana* leaves using an induction buffer (10 mM MES, pH 5.8, 10 mM $MgCl_2$, and 100 mM acetosyringone). After 72 h, 1 mM D-luciferin was smeared on the infiltrated *N. benthamiana* leaves, and the luminescence signals were photographed using a Tanon-5200 Chemiluminescent Imaging System. Disks were punched from infiltrated leaves and then quantified the luciferase activity using the luciferase reporter gene assay kit by Promega Glomax system.

BiFC and co-localization assays

The coding region of FgEC10 was fused into the pCambia1300-YFPC vector, and the *TaFAH* coding sequence was cloned into the pCambia1300-YFPN vector. The fusion vectors FgEC10-YFPC and TaFAH-YFPN were transformed into *A. tumefaciens* strain GV3101 and transiently co-expressed in *N. benthamiana* leaves. After 48 h, the GFP fluorescence signals in the infiltrated leaves were observed using a confocal microscope.

To determine the co-localization between FgEC10/TaPSMD12 and TaFAH, the coding sequence of *FgEC10* or *TaPSMD12* was fused into the pCambia1300-GFP vector, and the *TaFAH* coding sequence was cloned into the pCambia1300-mCherry vector. *A. tumefaciens* strains GV3101 containing the fused constructs were co-infiltrated into *N. benthamiana* leaves. The GFP and mCherry signals were detected by confocal microscopy.

Co-immunoprecipitation (Co-IP) assay

The coding sequences of *FgEC10* and *TaPSMD12* were subcloned into pCambia1300-GFP to form pCambia1300-FgEC10-GFP and pCambia1300-TaPSMD12-GFP vectors, respectively. The *TaFAH* sequence was fused to the pCambia1300-Flag vector to produce pCambia1300-TaFAH-Flag. All constructs were introduced into *A. tumefaciens* strain GV3101 and co-expressed in *N. benthamiana* leaves. After 72 h, total protein was extracted using Co-IP buffer (50 mM Tris-HCl, pH 7.4, 150 mM NaCl, 5 mM $MgCl_2$, 10% glycerol, 0.1% NP40, 1 mM PMSF, and protease inhibitor cocktail). Total protein extracts were incubated with GFP-Trap beads (Sangon Biotech, Shanghai, China) at 4 °C for 2 h. The incubated beads were washed thrice with the same lysis buffer and boiled in SDS protein loading buffer. The samples were separated using a 10% SDS-PAGE gel and subjected to immunoblot analyses using monoclonal anti-GFP (TRANSGEN, HT801-02, 1:5000 dilution) or anti-Flag (Sigma-Aldrich, F1804, 1:5000 dilution) antibodies.

In vitro pulldown assay

The pGEX-4T, pMBP-c5X, and pET28a vectors were used to express the GST-, MBP-, and HIS-tagged proteins, respectively. Recombinant pGEX-4T-TaFAH, pMBP-FgEC10, and pET28a-TaPSMD12 were introduced into *E. coli* BL21 (DE3). Cultures were induced with 0.5 mM isopropylthio galactosidases (IPTG) at 16 °C for 16 h with shaking at 200 rpm.

For verifying the interactions of TaFAH-FgEC10 or TaFAH-TaPSMD12, glutathione agarose beads (Cytiva) were first added to the *E. coli* crude extract containing the GST-TaFAH recombinant protein at 4 °C for 2 h. After removing the supernatant, the beads were washed three times with PBS buffer and mixed with MBP-FgEC10 or HIS-TaPSMD12 crude extract at 4 °C for 2 h. Then the beads were enriched, washed with PBS buffer, and heated at 100 °C in SDS loading buffer for 5 min for the western blot analysis using anti-GST, anti-MBP, or anti-HIS antibodies.

To detect the role of FgEC10 in the interaction between TaFAH and TaPSMD12, recombinant MBP-FgEC10, GST-TaFAH, and HIS-TaPSMD12 proteins were first purified. Then, equal amounts of GST-TaFAH and HIS-TaPSMD12 fusion proteins were co-incubated with different amounts of MBP-FgEC10 protein (1×, 5×, 10×, and 20×) before mixing with MBP beads.

Protein degradation assays

The in vitro protein degradation assays were performed as described previously[22,61]. In brief, 3.5 μg purified GST-TaFAH was co-incubated with a total of 100 μL protein extracted from wheat flowering heads for 0, 15, 30, 45, and 60 min before mixing with or without 100 μM proteasome inhibitor MG132. The GST-TaFAH was subjected to immunoblot analyses with anti-GST antibody. Wheat actin protein, the endogenous reference, was detected using an anti-actin antibody.

In vitro ubiquitination assay

The TaFAH were cloned into the pMBP-c5X vector and expression was induced. The fusion proteins were incubated with MBP beads for two hours and washed three times with column buffer (20 mM Tris-HCl, pH 7.4, 200 mM NaCl, and 1 mM EDTA). An equal amount of beads was then incubated with reaction buffer containing total protein of JM22, 5 mM ATP, 100 μM MG132, and FgEC10 or TaPSMD12 protein. After 30 min, the beads were washed with column buffer, and the fusion protein was eluted with column buffer containing 10 mM maltose. The

products were subjected to Western blot detection using anti-MBP and anti-UBQ (Agrisera, AS08307A) antibodies.

Acetoacetate content detection

The fusion constructs pCambia-TaFAH-Flag and pCambia-FgEC10-GFP were introduced into *A. tumefaciens* strain GV3101 and co-expressed in *N. benthamiana* leaves. After 24 h, 10 μM MG132 was infiltrated into the same sites. The product, acetoacetic acid, was detected using an acetoacetic acid (AcAc) content detection kit (HKSBC5070) according to the instruction manual.

Generation of transgenic wheat plants

The coding sequence of *TaFAH* was cloned into the pWMB110 vector driven by the *Ubi* promoter for overexpression. A 300-bp fragment of *TaFAH* was cloned into the vector pWMB110-RNAi in both antisense and sense orientations for silencing. The resulting constructs, pWMB110-TaFAH and pWMB110-RNAi-TaFAH, were transformed into the wheat cultivar Fielder using the *A. tumefaciens* strain EHA105. The phosphinothricin acetyltransferase gene bar was used as the selective marker. The expression levels of *TaFAH* in the T0 and T1 generations were determined using RT-qPCR. Transgenic plants with over 2-fold increase or reduction in *TaFAH* expression were selected for infection assays with *F. graminearum* as described above.

Bioinformatic analysis

The signal peptide of effector candidates was predicted by SignalP 4.1[62] and TargetP 2.0[63]. Identification of FgEC10 homologs was performed against the NCBI database based on BLASTp searches. Unrooted phylogenetic trees were constructed using MEGA 7 with the neighbor-joining method[64].

For RNA-seq analysis, wheat leaves were collected at the booting stage, and RNA sequencing was conducted by Novogene Co., Ltd. (Beijing, China) using an Illumina Novaseq6000 sequencer with paired-end 150 bp reads. Raw reads were cleaned and mapped to the wheat reference genome. The transcripts were quantified using the Cufflinks software (version 1.3.1). To describe the relative abundance of transcripts and create differential expression values (|log2 fold change| > 1 and false discovery rate [FDR] 0.05), fragments per kilobase of transcript per million mapped reads (FPKM) were used. The R package clusterProfiler was used to perform KEGG pathway and GO enrichment analyses based on the Benjamin–Hochberg correction.

Untargeted metabolomics analysis

Wheat heads samples from three overexpressing lines (*TaFAH*-OE 1, 3, 4) or three RNA silencing lines (*TaFAH*-RNAi 1, 2, 5) were mixed and then used for metabolomics analysis in six biological replicates per treatment. Samples were ground using a mortar and pestle. Approximately 60 mg of the lyophilized powder was mixed with 600 μL methanol-water (7:3 (v/v), including mixed internal standard, 4 μg/mL). After grinding at 60 Hz for 2 min, the mixtures were incubated at 4 °C overnight and centrifuged at 12,000 × *g* for 10 min, and the extract was filtered with a 0.22 μm organic phase pinhole filter. Waters ACQUITY UPLC I-Class plus/Thermo QE was used to acquire LC-MS spectra on data-dependent acquisition (DDA). In this mode, data collection conditions were set as follows: Capillary Temperature as 320 °C, Aux gas heater temperature as 350 °C, Aux gas flow rate as 8, Spray Voltage as 3800 V or −3000 V in positive or negative modes, respectively. Raw metabolomic data underwent preprocessing using Progenesis QI v3.0 software (Waters Corporation, Newcastle, UK), including baseline filtering, nonlinear dynamic processing, spectral integration, retention time correction, peak alignment, and normalization, with parameters configured as follows: precursor ion tolerance: 5 ppm (for HMDB and Lipidmaps databases)/10 ppm (for LuMet-Plant and METLIN databases); product ion tolerance: 10 ppm (HMDB and Lipidmaps)/20 ppm (LuMet-Plant and METLIN).

For GC-MS, 150 μL of supernatant was transferred to a glass-derived vial, and the sample was dried in a centrifugal concentrator. Then, 80 μL methicillin hydrochloride pyridine solution (15 mg/mL) was added to the glass-derived vial and incubated at 37 °C for 60 min for the oxime reaction to occur. The samples were added to 50 μL BSTFA derivatization reagent and 20 μL hexane and incubated at 70 °C for 60 min. The samples were incubated at room temperature for 30 min and detected using an Agilent 8890-5977B with the following parameters: Electron bombardment ion source (EI), ion source temperature 230 °C, quadrupole temperature 150 °C, electron energy 70 eV. Scanning mode is full scanning mode (SCAN), quality scanning range: m/z 50–500. The GC-MS raw data format is converted by the AnalysisBaseFileConverter software, which utilizes the ABF basic file format to facilitate the expeditious retrieval of data. Subsequent to preprocessing, the MS-DIAL software v4.24 is imported by means of the chromatographic peak "model". This is an algorithm that is employed to extract background noise through the retention time. The metabolites showing statistically significant changes were obtained at the level of fold change > 1.2, VIP > 1, and $P < 0.05$.

Targeted metabolomics analysis of amino acids

For the purpose of detecting the accumulation of acidic amino acids in transgenic wheat heads, samples were obtained as outlined above. The homogenization of an appropriate quantity of the specimen with 400 μL of a pre-chilled (4 °C) methanol-water solution (v/v 4:1, containing 0.1% formic acid) was then conducted. The mixture was equilibrated at −20 °C for 2 min, followed by mechanical grinding at 60 Hz for two min. The homogenate was then vortexed for one minute, ultrasonicated in an ice-water bath for ten minutes, and then subjected to centrifugation at 12,000 rpm (4 °C) for a further ten minutes. Thereafter, 200 μL of the resulting pellet was collected and evaporated to dryness. The residual pellet was then subjected to a second extraction with 200 μL of the same pre-chilled methanol-water solution, repeating the vortexing, ultrasonication, and centrifugation steps under identical conditions. The combined dried extracts were then reconstituted in 320 μL of acetonitrile-water (v/v 3:1), followed by 30 s of vortex mixing and five min of ice-water bath ultrasonication. Following a final centrifugation at 13,000 rpm (4 °C, ten min), the resultant pellet was filtered through a 0.22 μm organic phase syringe filter into amber HPLC vials for subsequent LC-MS analysis using AB Sciex Qtrap 5500/Nexera UHPLC LC-30A. The mass spectrometry analysis was performed with the following optimized settings: The curtain gas was maintained at 35 psi, and collision-activated dissociation (CAD) was set to medium. Electrospray ionization operated at spray voltages of +5500 V (positive ion mode) and −4500 V (negative ion mode), with an ion source temperature of 450 °C. The column temperature was stabilized at 40 °C. The nebulizer gas (Gas1) and auxiliary heating gas (Gas2) pressures were both calibrated to 55 psi. The raw data was processed with MRMPro software, which employs default parameters for the automatic identification and integration of each MRM transition.

Fungal inhibition and exogenous application of amino acid assays

The amino acids were dissolved in distilled water and diluted to a concentration of 10, 30, 50, and 80 mM using PDA. Each plate was inoculated with a 5 mm diameter mycelial plug of *F. graminearum* and incubated in the dark at 25 °C for 4 days. For each plate, two colony diameters were measured along perpendicular axes.

At the wheat flowering stage, a 20 mM solution of amino acids was sprayed onto wheat heads (cv. Fielder) over the course of two consecutive sessions, separated by 48 h. Ten microlitres of *F. graminearum* conidia were injected into the spikelet. The inoculated wheat heads were subsequently bagged to preserve moisture for 48 h. The number of infected spikelets was then observed and recorded at 10 dpi.

At the wheat seedling stage, 100 ml of 20 mM amino acids was poured into the small pot in which the wheat seedlings were planted

for 10 days. Then, 6 days later, 100 μL of *F. graminearum* conidia were injected into the base of the wheat stem. The experiment consisted of three independent replicates with at least 9 plants each.

Statistics and reproducibility

Tanon-5200 Chemiluminescent Imaging System (Tanon Science & Technology Co., Ltd) was used for WB data collection. All confocal micrographs were collected by Leica TCS SP8. All representative experiments, such as micrographs and co-immunoprecipitations, were performed at least twice with similar results. GraphPad Prism 9.0 and Microsoft Office Excel were used for statistical analysis. Statistics were performed using one-way analysis of variance (ANOVA) tests or unpaired one-tailed Student's *t*-test. Data are reported as the mean ± SD. All analyses were performed on a minimum of three biological replicates unless otherwise specified. No data were excluded from the analyses. The investigators were not blinded to allocation during experiments and outcome assessment.

Reporting summary

Further information on research design is available in the Nature Portfolio Reporting Summary linked to this article.

Data availability

The RNA-seq data generated in this study has been deposited in the NCBI Sequence Read Archive database under accession code PRJNA1070554. The metabolomic data generated in this study have been deposited in the MassIVE database under accession code MSV000097681 [https://massive.ucsd.edu/ProteoSAFe/dataset.jsp?task=1c7b1a3bc8004fa1882263665afad1aa] and MSV000097684 [https://massive.ucsd.edu/ProteoSAFe/dataset.jsp?task=a76e498af0124060a13684428c39f8d4]. All data supporting the findings of this work are available in the paper, Supplementary Information files, and the repository platform. Raw images underlying Figs. 6b, d, and 8c are available via https://doi.org/10.6084/m9.figshare.29178803. Source data are provided with this paper.

References

1. Chen, Y., Kistler, H. C. & Ma, Z. *Fusarium graminearum* trichothecene mycotoxins: biosynthesis, regulation, and management. *Annu. Rev. Phytopathol.* **57**, 15–39 (2019).
2. McCormick, S. P., Stanley, A. M., Stover, N. A. & Alexander, N. J. Trichothecenes: from simple to complex mycotoxins. *Toxins* **3**, 802–814 (2011).
3. Li, G. et al. Mutation of a histidine-rich calcium-binding-protein gene in wheat confers resistance to *Fusarium* head blight. *Nat. Genet.* **51**, 1106–1112 (2019).
4. Su, Z. et al. A deletion mutation in TaHRC confers Fhb1 resistance to *Fusarium* head blight in wheat. *Nat. Genet.* **51**, 1099–1105 (2019).
5. Wang, H. et al. Horizontal gene transfer of Fhb7 from fungus underlies Fusarium head blight resistance in wheat. *Science* **368**, eaba5435 (2020).
6. Brown, N. A., Evans, J., Mead, A. & Hammond-Kosack, K. E. A spatial temporal analysis of the *Fusarium graminearum* transcriptome during symptomless and symptomatic wheat infection: transcriptome of symptomless *Fusarium* infection. *Mol. Plant Pathol.* **18**, 1295–1312 (2017).
7. Jia, L. J. et al. A linear nonribosomal octapeptide from *Fusarium graminearum* facilitates cell-to-cell invasion of wheat. *Nat. Commun.* **10**, 922 (2019).
8. Son, H. et al. A Phenome-based functional analysis of transcription factors in the cereal head blight fungus, *Fusarium graminearum*. *PLoS Pathog.* **7**, e1002310 (2011).
9. Wang, C. et al. Functional analysis of the Kinome of the wheat scab fungus *Fusarium graminearum*. *PLoS Pathog.* **7**, e1002460 (2011).
10. Yun, Y. et al. Functional analysis of the *Fusarium graminearum* phosphatome. *New Phytol.* **207**, 119–134 (2015).
11. Giraldo, M. C. & Valent, B. Filamentous plant pathogen effectors in action. *Nat. Rev. Microbiol.* **11**, 800–814 (2013).
12. Dodds, P. N. & Rathjen, J. P. Plant immunity: towards an integrated view of plant-pathogen interactions. *Nat. Rev. Genet.* **11**, 539–548 (2010).
13. Tsuda, K. & Katagiri, F. Comparing signaling mechanisms engaged in pattern-triggered and effector-triggered immunity. *Curr. Opin. Plant Biol.* **13**, 459–465 (2010).
14. Dou, D. & Zhou, J. M. Phytopathogen effectors subverting host immunity: different foes, similar battleground. *Cell Host Microbe* **12**, 484–495 (2012).
15. Dangl, J. L., Horvath, D. M. & Staskawicz, B. J. Pivoting the plant immune system from dissection to deployment. *Science* **341**, 746–751 (2013).
16. de Jonge, R. et al. Conserved fungal LysM effector Ecp6 prevents chitin-triggered immunity in plants. *Science* **329**, 953–955 (2010).
17. Zheng, X. et al. *Ustilaginoidea virens* secretes a family of phosphatases that stabilize the negative immune regulator OsMPK6 and suppress plant immunity. *Plant Cell* **34**, 3088–3109 (2022).
18. Yang, B. et al. The *Phytophthora sojae* RXLR effector Avh238 destabilizes soybean type2 GmACSs to suppress ethylene biosynthesis and promote infection. *New Phytol.* **222**, 425–437 (2018).
19. Yang, F. et al. Secretomics identifies *Fusarium graminearum* proteins involved in the interaction with barley and wheat: *Fusarium graminearum* secretome. *Mol. Plant Pathol.* **13**, 445–453 (2012).
20. Blümke, A. et al. Secreted fungal effector lipase releases free fatty acids to inhibit innate immunity-related callose formation during wheat head infection. *Plant Physiol.* **165**, 346–358 (2014).
21. Qi, P. F. et al. Functional analysis of FgNahG clarifies the contribution of salicylic acid to wheat (*Triticum aestivum*) resistance against *Fusarium* head blight. *Toxins* **11**, 59 (2019).
22. Jiang, C. et al. An orphan protein of *Fusarium graminearum* modulates host immunity by mediating proteasomal degradation of TaSnRK1α. *Nat. Commun.* **11**, 4382 (2020).
23. Tsuchiya, H. et al. In vivo ubiquitin linkage-type analysis reveals that the Cdc48-Rad23/Dsk2 axis contributes to K48-linked chain specificity of the proteasome. *Mol. Cell* **66**, 488–502 (2017).
24. Daniel, M., Rosa, V. & Pascual, S. Two-hybrid analysis identifies PSMD11, a non-ATPase subunit of the proteasome, as a novel interaction partner of AMP-activated protein kinase. *Int. J. Biochem. Cell Biol.* **41**, 2431–2439 (2009).
25. Kish-Trier, E. & Hill, C. P. Structural biology of the proteasome. *Annu. Rev. Biophys.* **42**, 29–49 (2013).
26. Ashida, H., Kim, M. & Sasakawa, C. Exploitation of the host ubiquitin system by human bacterial pathogens. *Nat. Rev. Microbiol.* **12**, 399–413 (2014).
27. Lin, Y. H. & Machner, M. P. Exploitation of the host cell ubiquitin machinery by microbial effector proteins. *J. Cell Sci.* **130**, 1985–1996 (2017).
28. Wang, Z. et al. A *Phytophthora infestans* RXLR effector targets a potato ubiquitin-like domain-containing protein to inhibit the proteasome activity and hamper plant immunity. *New Phytol.* **238**, 781–797 (2023).
29. Park, C. H. et al. The *Magnaporthe oryzae* effector AvrPiz-t targets the RING E3 ubiquitin ligase APIP6 to suppress pathogen-associated molecular pattern-triggered immunity in rice. *Plant Cell* **24**, 4748–4762 (2012).
30. Park, C. H. et al. The E3 ligase APIP10 connects the effector AvrPiz-t to the NLR receptor Piz-t in rice. *PLoS Pathog.* **12**, e1005529 (2016).
31. IWGSC. A chromosome-based draft sequence of the hexaploid bread wheat (*Triticum aestivum*) genome. *Science* **345**, 6194 (2014).

32. Win, J. et al. Effector biology of plant-associated organisms: concepts and perspectives. *Cold Spring Harb. Symp. Quant. Biol.* **77**, 235–247 (2012).
33. Wang, N. et al. Inactivation of a wheat protein kinase gene confers broad-spectrum resistance to rust fungi. *Cell* **185**, 2961–2974.e19 (2022).
34. Li, G. B. et al. Overproduction of OsRACK1A, an effector-targeted scaffold protein promoting OsRBOHB-mediated ROS production, confers rice floral resistance to false smut disease without yield penalty. *Mol. Plant* **15**, 1790–1806 (2022).
35. Chen, L. Q. et al. Sugar transporters for intercellular exchange and nutrition of pathogens. *Nature* **468**, 527–532 (2010).
36. Oliva, R. et al. Broad-spectrum resistance to bacterial blight in rice using genome editing. *Nat. Biotechnol.* **37**, 1344–1350 (2019).
37. Shang, S. P. et al. *Fusarium graminearum* effector FgEC1 targets wheat TaGF14b protein to suppress TaRBOHD-mediated ROS production and promote infection. *J. Integr. Plant Biol.* **66**, 2288–2303 (2024).
38. Collins, G. A. & Goldberg, A. L. The logic of the 26S proteasome. *Cell* **169**, 792–806 (2017).
39. Liu, T. et al. The 26S proteasome regulatory subunit GmPSMD promotes resistance to *Phytophthora sojae* in soybean. *Front. Plant Sci.* **12**, 513388 (2021).
40. McHale, L., Tan, X., Koehl, P. & Michelmore, R. W. Plant NBS-LRR proteins: adaptable guards. *Genome Biol.* **7**, 212 (2006).
41. Wang, R., He, F., Ning, Y. & Wang, G. L. Fine-tuning of RBOH-mediated ROS signaling in plant immunity. *Trends Plant Sci.* **25**, 1060–1062 (2020).
42. Vaghela, B., Vashi, R., Rajput, K. & Joshi, R. Plant chitinases and their role in plant defense: a comprehensive review. *Enzyme Microb. Tech.* **159**, 110055 (2022).
43. Han, C. Y. et al. Disruption of fumarylacetoacetate hydrolase causes spontaneous cell death under short-day conditions in *Arabidopsis*. *Plant Physiol.* **162**, 1956–1964 (2013).
44. Hildebrandt, T. M., Nesi, A. N., Araújo, W. L. & Braun, H. P. Amino acid catabolism in plants. *Mol. Plant* **8**, 1563–1579 (2015).
45. Jones, J. D. G. & Dangl, J. L. The plant immune system. *Nature* **444**, 323–329 (2006).
46. Rafiqi, M., Ellis, J. G., Ludowici, V. A., Hardham, A. R. & Dodds, P. N. Challenges and progress towards understanding the role of effectors in plant-fungal interactions. *Curr. Opin. Plant Biol.* **15**, 477–482 (2012).
47. Fu, H., Reis, N., Lee, Y., Glickman, M. H. & Vierstra, R. D. Subunit interaction maps for the regulatory particle of the 26S proteasome and the COP9 signalosome. *EMBO J.* **20**, 7096–7107 (2001).
48. Book et al. The RPN5 subunit of the 26s proteasome is essential for gametogenesis, sporophyte development, and complex assembly in *Arabidopsis*. *Plant Cell* **21**, 460–478 (2009).
49. Zhang, Y. et al. The extra-pathway interactome of the TCA cycle: expected and unexpected metabolic interactions. *Plant Physiol.* **177**, 966–979 (2018).
50. Kadotani, N., Akagi, A., Takatsuji, H., Miwa, T. & Igarashi, D. Exogenous proteinogenic amino acids induce systemic resistance in rice. *BMC Plant Biol.* **16**, 60 (2016).
51. Wang, X. et al. Amino acid fertilizer strengthens its effect on crop yield and quality by recruiting beneficial rhizosphere microbes. *J. Sci. Food Agric.* **103**, 5970–5980 (2023).
52. Zhao et al. Targeted and untargeted metabolomics profiling of wheat reveals amino acids increase resistance to *Fusarium* head blight. *Front. Plant Sci.* **12**, 762605 (2021).
53. Asai, T. et al. MAP kinase signalling cascade in *Arabidopsis* innate immunity. *Nature* **415**, 977–983 (2002).
54. Pitzschke, A., Schikora, A. & Hirt, H. MAPK cascade signalling networks in plant defence. *Curr. Opin. Plant Biol.* **12**, 421–426 (2009).
55. Zhang, J. et al. A *Pseudomonas syringae* effector inactivates MAPKs to suppress PAMP-induced immunity in plants. *Cell Host Microbe* **1**, 175–185 (2007).
56. Zhang, Z. et al. Disruption of PAMP-induced MAP kinase cascade by a *Pseudomonas syringae* effector activates plant immunity mediated by the NB-LRR protein SUMM2. *Cell Host Microbe* **11**, 253–263 (2012).
57. Chuma, I. et al. Multiple translocation of the avr-pita effector gene among chromosomes of the rice blast fungus *Magnaporthe oryzae* and related species. *PLoS Pathog.* **7**, e1002147 (2011).
58. Qiao, Y. et al. SPL28 encodes a clathrin-associated adaptor protein complex 1, medium subunit (AP1M1) and is responsible for spotted leaf and early senescence in rice (*Oryza sativa*). *New Phytol.* **185**, 258–274 (2010).
59. Pecrix, Y. et al. Sunflower resistance to multiple downy mildew pathotypes revealed by recognition of conserved effectors of the oomycete *Plasmopara halstedii*. *Plant J.* **97**, 730–748 (2019).
60. Catlett, N. L., Lee, B.-N., Yoder, O. C. & Turgeon, B. G. Split-marker recombination for efficient targeted deletion of fungal genes. *Fungal Genet. Rep.* **50**, 9–11 (2003).
61. Kong, L. et al. Degradation of the ABA co-receptor ABI1 by PUB12/13 U-box E3 ligases. *Nat. Commun.* **6**, 8630 (2015).
62. Nielsen, H. Predicting secretory proteins with SignalP. *Methods Mol. Biol.* **1611**, 59–73 (2017).
63. Armenteros, J. J. A. et al. Detecting sequence signals in targeting peptides using deep learning. *Life Sci. Alliance* **2**, e201900429 (2019).
64. Kumar, S., Stecher, G. & Tamura, K. MEGA7: molecular evolutionary genetics analysis version 7.0 for Bigger datasets. *Mol. Biol. Evol.* **33**, 1870–1874 (2016).

Acknowledgements

We thank Prof. Ke Wang at Institute of Crop Sciences, Chinese Academy of Agricultural Sciences for providing pWMB110 plasmid, and thank Prof. Huawei Zheng at Minjiang University for providing PH-1 strain. This work was supported by grants from the Basic Research Center for Agricultural Frontiers and Interdisciplinary Sciences (BRC-AFIS), Innovation Program of Chinese Academy of Agricultural Sciences (CAAS-BRC-AFIS-2025-02), National Natural Science Foundation of China (Grant 32402475), and the Science, Technology, and Innovation Commission of Shenzhen Municipality.

Author contributions

S.S. and C.-J.Z. designed the experiments; S.S., Y.H., R.Z., H.L., Y.F., Q.H., Y.J.F., Y.W., and X.Z. performed the experiments; S.S., P.W., X.X., and C.-J.Z. analyzed the data; S.S. and C.-J.Z. wrote the manuscript.

Competing interests

The authors declare no competing interests.

Additional information

Supplementary information The online version contains supplementary material available at https://doi.org/10.1038/s41467-025-60736-y.

Correspondence and requests for materials should be addressed to Cui-Jun Zhang.

Peer review information *Nature Communications* thanks Qian Xu and the other anonymous reviewer(s) for their contribution to the peer review of this work. [A peer review file is available].